Fuzzy logic based power management strategy of a multi-MW doubly-fed induction generator wind turbine with battery and ultracapacitor

Raúl Sarrias-Mena, Luis M. Fernández-Ramírez, Carlos Andrés García-Vázquez, Francisco Jurado

Published in:
Energy, vol. 70, pp. 561-576

DOI (link to publication from Publisher):
https://doi.org/10.1016/j.energy.2014.04.049

Publication date:
2014

Document Version:
Accepted version

Citation for published version:
R. Sarrias-Mena, L. M. Fernández-Ramírez, C. A. García-Vázquez, F. Jurado, "Fuzzy logic based power management strategy of a multi-MW doubly-fed induction generator wind turbine with battery and ultracapacitor," *Energy*, vol. 70, pp. 561-576, 01-Jun-2014. https://doi.org/10.1016/j.energy.2014.04.049.

Elsevier Editorial System(tm) for Energy
Manuscript Draft

Manuscript Number: EGY-D-13-01748R2

Title: Fuzzy logic based power management strategy of a multi-MW DFIG wind turbine with battery and ultracapacitor

Article Type: Full Length Article

Keywords: Energy storage; DFIG wind turbine; fuzzy control; power management.

Corresponding Author: Dr. Luis M. Fernández, Ph. D.

Corresponding Author's Institution: University of Cadiz

First Author: Raúl Sarrias, M.Sc.

Order of Authors: Raúl Sarrias, M.Sc.; Luis M. Fernández, Ph. D.; Carlos Andres García, Ph.D.; Francisco Jurado, Ph.D.

Abstract: Integrating energy storage systems (ESS) with wind turbines results to be an interesting option of improving the grid integration capability of wind energy. This paper presents and evaluates a wind hybrid system consisting of a 1.5 MW doubly-fed induction generator (DFIG) wind turbine and double battery-ultracapacitor ESS. Commercially available components are used in this wind hybrid system. A novel supervisory control system (SCS) is designed and implemented, which is responsible for setting the active and reactive power references for each component of the hybrid system. A fuzzy logic controller, taking into account the grid demand, power generation prediction, actual DFIG power generation and state-of-charge (SOC) of the ESSs, sets the active power references. The reactive power references are proportionally delivered to each element regarding their current limitations in the SCS. The appropriate control of the power converters allows each power source to achieve the operation defined by the SCS. The wind hybrid system and SCS are assessed by simulation under wind fluctuations, grid demand changes, and grid disturbances. Results show an improved performance in the overall response of the system with the implementation of the SCS.

Highlights:

- We study a wind hybrid system based on DFIG wind turbine, battery and ultracapacitor.
- A novel supervisory control system based on fuzzy logic is designed and implemented.
- The control improves the system response under different operating conditions.

Fuzzy logic based power management strategy of a multi-MW DFIG wind turbine with battery and ultracapacitor

Raúl Sarrias-Mena [1], Luis M. Fernández-Ramírez [1,*], Carlos Andrés García-Vázquez [1], Francisco Jurado [2]

[1] *Research Group in Electrical Technologies for Sustainable and Renewable Energy (PAIDI-TEP-023), Department of Electrical Engineering, University of Cadiz, 11202 EPS Algeciras, Algeciras (Cadiz), Spain*

[2] *Research Group in Research and Electrical Technology (PAIDI-TEP-152), Department of Electrical Engineering, University of Jaen, 23700 EPS Linares, Linares (Jaen), Spain*

Abstract

Integrating energy storage systems (ESS) with wind turbines results to be an interesting option of improving the grid integration capability of wind energy. This paper presents and evaluates a wind hybrid system consisting of a 1.5 MW doubly-fed induction generator (DFIG) wind turbine and double battery-ultracapacitor ESS. Commercially available components are used in this wind hybrid system. A novel supervisory control system (SCS) is designed and implemented, which is responsible for setting the active and reactive power references for each component of the hybrid system. A fuzzy logic controller, taking into account the grid demand, power generation prediction, actual DFIG power generation and state-of-charge (SOC) of the ESSs, sets the active power references. The reactive power references are proportionally delivered

* Corresponding author. Tel.: +34 956 028166; fax: +34 956 028014.
E-mail addresses: raul.sarrias@uca.es (R. Sarrias-Mena), luis.fernandez@uca.es (L. M. Fernández-Ramírez), carlosandres.garcia@uca.es (C. A. García-Vázquez), fjurado@ujaen.es (F. Jurado).

to each element regarding their current limitations in the SCS. The appropriate control of the power converters allows each power source to achieve the operation defined by the SCS. The wind hybrid system and SCS are assessed by simulation under wind fluctuations, grid demand changes, and grid disturbances. Results show an improved performance in the overall response of the system with the implementation of the SCS.

Keywords.

Energy storage; DFIG wind turbine; fuzzy control; power management.

Nomenclature.

Acronyms

BESS – Battery energy storage system.

DFIG – Doubly-fed induction generator.

ESS – Energy storage system.

GSC – DFIG grid side converter.

MPPT – Maximum power point tracking.

PCC – Point of common coupling.

RSC – DFIG rotor side converter.

SCS – Supervisory control system.

SOC – State-of-charge of the energy storage system.

UC – Ultracapacitor.

VRLA – Valve-regulated lead-acid.

Parameters

A – Swept area of the rotor disk.

C – Capacity of the DFIG DC link capacitor.

CAP – Maximum battery capacity.

C_p – Power coefficient of the wind turbine.

C_{UC} – UC capacity.

E_{batt} – Battery no-load voltage.

i_{batt} – Instantaneous battery current.

i_{dr}, i_{qr} – Direct and quadrature components of the rotor currents.

i_{ds}, i_{qs} – Direct and quadrature components of the stator currents.

i_{dg}, i_{qg} – Direct and quadrature components of the current at the AC side of the GSC.

I_s, I_r – Stator and rotor currents.

I_{UC} – UC series branch current.

L_r, R_r – Rotor windings electrical inductance and resistance.

L_s, R_s – Stator windings electrical inductance and resistance.

L_M – DFIG magnetizing inductance.

p – Number of DFIG pole pairs.

P_{conv}, Q_{conv}, S_{conv} – Active, reactive and apparent power of the AC/DC power converters.

$P_{exchange}$ – Compensating power between UC and BESS.

P_{dem}, Q_{dem} – Active and reactive grid power demand.

P_g – Total DFIG active power generation.

P_{gsc}, Q_{gsc} – Active and reactive power through the GSC of the DFIG.

P-$P_{BESS\ ref}$ – Primary active power reference for the BESS.

P-$P_{UC\ ref}$ – Primary active power reference for the UC.

P_r – Active power through the DFIG rotor windings.

P_s, Q_s – Active and reactive power through the DFIG stator windings.

Q_{s_ref} – Reactive power reference for the DFIG stator.

$Q_{s\_con\_lim}$ – Reactive power consumption limit for the DFIG stator.

$Q_{con\_lim\_total}$ – Total reactive power consumption limit for the hybrid system.

R_i – Battery internal resistance.

R_{UC} – UC internal resistance.

slip – DFIG rotor slip.

S_{s_Ir} – Stator apparent power according to the limit rotor current.

S_{s_Vr} – Stator apparent power according to the limit rotor voltage.

S_{s_Is} – Stator apparent power according to the limit stator current.

SOC_{BESS} – Battery state-of-charge.

SOC_{UC} – UC state-of-charge.

T_e – DFIG electromechanical torque.

T_{wt} – Wind turbine mechanical torque.

U_{batt} – Battery output voltage.

U_c – Voltage at the DC link capacitor of the DFIG.

U_s, U_r – Stator and rotor voltage.

u_{dg}, u_{qg} – Direct and quadrature components of the voltage at the AC side of the GSC.

u_{dr}, u_{qr} – Direct and quadrature components of the rotor voltage.

u_{ds}, u_{qs} – Direct and quadrature components of the stator voltage.

U_{UC} – UC instantaneous voltage.

$U_{UC\ rated}$ – UC rated voltage.

U_{UC_0} – UC initial voltage.

v – Wind speed.

V_{B575} – Voltage at the output terminals of the hybrid system.

$V_{dc\ DFIG}$, $V_{dc\ BESS}$, $V_{dc\ UC}$ – DC bus voltage of the DFIG, BESS and UC power converter.

Z_s, Z_r, Z_m – Stator, rotor and mutual impedances.

Greek

θ – Blades pitch angle.

λ – Tip speed ratio.

ρ – Air density.

φ_{dr}, φ_{qr} – Direct and quadrature components of the magnetic flux linkages for rotor.

φ_{ds}, φ_{qs} – Direct and quadrature components of the magnetic flux linkages for stator.

ω – DFIG synchronous speed.

ω_r – DFIG angular speed.

Φ – Rotor radius.

1. Introduction

Coupled operation of ESSs together with wind turbines is nowadays a feasible way to reduce intermittency, unpredictability and fluctuations on wind power generation [1-4]. If these issues are addressed, connection to grid of large wind farms becomes safer and more reliable. Due to the recent commercialization of wind turbines in the range of several megawatts equipped with ESS [5], the modeling and control of such devices becomes more necessary.

Different energy storage technologies are available for these purposes. A complete and up-to-date evaluation on the most relevant technologies is presented in [6]. Each of them presents particular characteristics that make them more suitable for a specific application. In this regard, ultracapacitors (UCs) typically show a fast response and low energy density, thus being able to complete charge and discharge cycles within a few minutes or seconds [7,8]. On the other hand, electrochemical batteries are more adequate for longer charge/discharge periods, since their higher capacity prevails over

their response time, which is slower than in the ultracapacitors [8]. Therefore, the wind hybrid system proposed in this paper aims to take advantage of the most remarkable characteristics of both devices.

Wind speed prediction is also a valuable tool for the operation of large grid-connected wind farms [9,10]. Accurate wind forecasts allow the estimation of future wind power generation in a particular location. This analysis can be carried out in different time scales for specific purposes. For instance, short-term estimations can help in the daily generation scheduling [11,12], which is of great importance from the grid operator point of view. In [11], the authors developed a hybrid wind speed forecasting model which achieved satisfactory accuracy with simple calculation process, thus easing its implementation on wind farms. In [12], a combined wind power and speed forecasting method for time-scales from minutes to an hour was presented. However, this model was not adequate for day-ahead prediction. An hourly average wind speed forecasting method was introduced in [13]. The proposed approach was proven valid for up to two-days-ahead predictions in some cases. Moreover, the authors used the power curve of a wind turbine to obtain the corresponding power generation forecast. This concept has been adopted in this paper, as it will be stated later on. The previous studies demonstrate the feasibility of performing time-ahead wind power prediction. Nonetheless, the implementation of a forecasting algorithm is not the goal of this paper, and the wind power prediction is considered given by an external system.

Fuzzy logic controllers show a remarkable flexibility in electric power applications. Their performance together with wind power generation and other renewable sources has been analyzed in the literature [14]. In [15], a fuzzy control was used to enhance wind power stability under fluctuating wind speed. Nonetheless, its combination with ESSs was not addressed. In [16], the authors showed the improvements achieved with

the integration of fuzzy logic and UC in a micro grid, compared to PI controllers. However, fuzzy logic and UC were evaluated separately, thus not studying the coupled application of both technologies. Some studies applied fuzzy logic controllers for power control and voltage regulation of wind turbines without any ESSs. Almeida et al. [17] compared PI with fuzzy system to control DFIG wind turbines in dynamic simulations, evaluating the stability behavior of a power system under disturbances. Despite reducing the possibilities of disconnection from the grid with the proposed control strategy, the absence of an ESS hinders improving the fault ride through of the wind turbine. Fuzzy logic controller was applied to direct power control strategies for a 2 MW DFIG wind turbine in [18]. These control structures are simple and robust under harmonically distorted and imbalanced grid voltages, but appropriate simulations according to dynamic stability studies are needed. Other authors considered the integration of fuzzy logic controllers into supervisory control schemes, providing an adequate energy management among the different elements in complex systems. Jerbi et al. [19] studied a fuzzy logic supervisory system for power control of a DFIG associated to a flywheel storage system in order to smooth the power fluctuations due to the random wind speed variations. Nevertheless, the study only considered the ESS to enhance power quality, and it did not investigate the system behavior under disturbances or fulfill grid requirements. On the other hand, some studies were focused on stand-alone hybrid power systems. Ansari and Velusami [20] proposed a dual mode linguistic hedge fuzzy logic controller for isolated wind-diesel hybrid power system with batteries. They represented the dynamic hybrid system with a linear model and studied its sensitivity and robustness. Similarly, Capizzi and Tina [21] implemented a fuzzy logic application to optimize the energy management of a photovoltaic and wind energy generation system. Although, the aim of their paper was to improve the long

energy performance of the system as a planning problem, they studied how the energy developed by the batteries was affected by the estimated SOC values. A similar function is proposed here for the fuzzy controller, since it operates as a part of the SCS in order to preserve the SOC of both ESSs between acceptable operational limits.

The goal of this paper focuses on the design and implementation of a novel supervisory control strategy for a hybrid wind turbine with two ESSs, i.e. battery energy storage system (BESS) and UC, in dynamic stability studies. A DFIG has been chosen as the wind turbine technology, due to its wide range of speed variation and its capacity to control both active and reactive power independently. The proposed control system exploits this possibility and works in different levels to generate the active and reactive power references for each device individually. The active power reference for the BESS and UC is firstly calculated regarding the actual DFIG power, a short-term wind power prediction converted to active power estimation through the power curve of the generator, and the grid demand, which can vary according to the grid operator requirements. Later, a fuzzy logic controller, which generates a compensating term depending on the state-of-charge (SOC) of the ESSs, modifies the primary reference. These compensated references are used as input in the control scheme of the corresponding controllers associated to the DC/DC power converters of each power source. A proportional dispatch is used to establish the reactive power reference of each device at the hybrid system, where their instantaneous limitations are considered in order to address the variable grid requirements. Both the active and reactive power references calculation schemes comprise the SCS of the wind hybrid system. The wind hybrid system and SCS are evaluated by simulation under different operating conditions, such as wind fluctuations, grid demand changes, and grid disturbances.

The paper is organized as follows. The global configuration of the wind hybrid system is presented in Section 2. In Section 3, the modeling of the main elements is described. The SCS is detailed in Section 4. Finally, the simulation results are shown and discussed in Section 5, and the conclusions are drawn in Section 6.

2. Wind hybrid system configuration

A wind hybrid system comprising a DFIG wind turbine and two different ESSs (BESS and UC) has been modeled in this work. The main advantage of using two different ESSs can be observed when they are demanded to address different purposes. Therefore, since their operating principle and dynamic response differ, it is reasonable to design a specific control strategy for each of them, according to the particular characteristics of both devices. In this hybrid system, BESS and UC have been chosen as ESSs, and their features have been thoroughly taken into account in the design of the control strategy.

As previously shown in the literature [22,23], the structure of a DFIG allows connecting an ESS within the partial-scale power converter of the generator. Nonetheless, if this configuration is chosen, the grid side converter (GSC) of the DFIG must be sized in order to manage the active power flow of the rotor side converter (RSC) plus the ESSs. Furthermore, only the reactive power through the GSC can be controlled.

On the other hand, it is possible to perform an improved control of the active and reactive power flow through the ESSs if they are connected at the DFIG output terminals. Moreover, this configuration can be implemented in both distributed and

aggregated wind farm – ESS schemes, since the sizing and control of the generator do not need to be modified.

Consequently, the configuration adopted in this paper consists of two ESSs connected at the generator output. As stated before, BESS and UC are used as ESSs. This structure requires power converters in order to couple the DC output power of the storage devices to the AC voltage at the connection point. Hence, a DC/DC and an AC/DC bidirectional converters with an intermediate DC bus become necessary for both ESSs, as shown in Fig. 1.

Fig. 1. Scheme of the wind hybrid turbine with double ESS (BESS and UC).

The use of power electronic converters also improves the control capability of the hybrid system output, since the power flow from/to the ESSs can be regulated in coordination with the wind power generator depending on the instantaneous operating conditions, as will be detailed in the description of the SCS.

3. Wind hybrid system model

In this section, the modeling of the most relevant devices integrated in the hybrid system is described. The General Electric 1.5 MW DFIG driven wind turbine [24] was considered here as the main power source, whereas the ESSs act as auxiliary power sources in order to support and secure an adequate power injection to grid. These devices were modeled according to commercially available components.

The hybrid system was modeled in MATLAB/Simulink using elements from the SimPowerSystem library. As the main contributions, the ESSs and DFIG wind turbine

were coupled together through bidirectional DC/DC and AC/DC power converters in order to establish the hybrid configuration. Moreover, the control strategies for all the energy sources were implemented, using well-known vector control for the RSC and GSC of the DFIG. Furthermore, a novel SCS was proposed and implemented to achieve the coordinated operation of the BESS, UC and DFIG power converters. This SCS is responsible for setting the active and reactive power references for all the components of the hybrid system, as will be detailed later on.

3.1. Wind turbine

The wind turbine model describes the mechanical behavior of the rotor and drive train. For this purpose, well known physical models were considered, such as the actuator disk theory [25] for the rotor and blades, and the two-mass dynamic model for the drive train [26]. Thus, the mechanical torque of the wind turbine, T_{wt}, can be calculated as in Eq. (1), and used as input to the DFIG.

$$T_{wt} = \frac{1}{2} \cdot \rho \cdot A \cdot \Phi \cdot v^2 \cdot \frac{C_p(\lambda,\theta)}{\lambda} \tag{1}$$

where ρ is the air density; A is the swept area of the rotor disk, which is proportional to the rotor radius Φ; v is the incoming wind speed; and C_p is the power coefficient, which is expressed as a function of both tip speed ratio λ (defined as the ratio between blade tip speed and wind speed) and the pitch angle of the rotor blades θ.

3.2. DFIG and converter control

The DFIG wind turbine is directly connected to grid through the stator windings of the generator, whereas the rotor windings exchange active and reactive power with the

grid through a bidirectional power converter that allows the variable speed operation of the generator.

In this paper, the fifth-order model of the DFIG is considered [27], which is composed of four differential equations for the stator and rotor voltage in the direct-quadrature (*dq*) reference frame rotating at synchronous speed, and the electromagnetic torque equation. Hence, the *d*-*q* components of the stator and rotor voltage are given by:

$$\begin{aligned} u_{ds} &= R_s \cdot i_{ds} + \frac{d}{dt}\varphi_{ds} - \omega \cdot \varphi_{qs} \\ u_{qs} &= R_s \cdot i_{qs} + \frac{d}{dt}\varphi_{qs} + \omega \cdot \varphi_{ds} \end{aligned} \tag{2}$$

$$\begin{aligned} u_{dr} &= R_r \cdot i_{dr} + \frac{d}{dt}\varphi_{dr} - \left(\omega - \omega_r\right) \cdot \varphi_{qr} \\ u_{qr} &= R_r \cdot i_{qr} + \frac{d}{dt}\varphi_{qr} + \left(\omega - \omega_r\right) \cdot \varphi_{dr} \end{aligned} \tag{3}$$

where u denotes voltage; i denotes current; ω is the DFIG synchronous speed; ω_r is the DFIG angular speed; φ represents magnetic flux; R denotes resistance; indexes d and q stand for the direct and quadrature components; and indexes s and r refer to stator and rotor respectively.

In Eqs. (2)-(3), the magnetic flux linkages for stator and rotor can be expressed as follows:

$$\begin{aligned} \varphi_{ds} &= L_s \cdot i_{ds} + L_M \cdot i_{dr} \\ \varphi_{qs} &= L_s \cdot i_{qs} + L_M \cdot i_{qr} \end{aligned} \tag{4}$$

$$\begin{aligned} \varphi_{dr} &= L_r \cdot i_{dr} + L_M \cdot i_{ds} \\ \varphi_{qr} &= L_r \cdot i_{qr} + L_M \cdot i_{qs} \end{aligned} \tag{5}$$

where index *M* stands for magnetizing; and *L* is inductance.

Finally, the electromechanical torque, T_e, is given by Eq. (6):

$$T_e = 1.5 \cdot p \cdot \left(\varphi_{ds} \cdot i_{qs} - \varphi_{qs} \cdot i_{ds} \right) \quad (6)$$

where *p* is the number of pole pairs in the DFIG.

The power converter consists of two back-to-back bridges (named RSC and GSC, according to their position in the DFIG scheme) linked by a DC bus. It was modeled as a PWM converter based on IGBT switches.

Vector control strategies were implemented in both the RSC and GSC (Fig. 2a and b respectively). The former regulates, independently by means of the *dq* rotor current and voltage, the total DFIG active power generation (P_g), as a sum of the stator and rotor power (namely P_s and P_r), and the stator reactive power (Q_s). These parameters can be obtained through Eqs. (7)-(10).

$$P_s = 1.5 \cdot \left(u_{ds} \cdot i_{ds} + u_{qs} \cdot i_{qs} \right) \quad (7)$$

$$P_r = 1.5 \cdot \left(u_{dr} \cdot i_{dr} + u_{qr} \cdot i_{qr} \right) \quad (8)$$

$$P_g = P_s + P_r \quad (9)$$

$$Q_s = 1.5 \cdot \left(u_{qs} \cdot i_{ds} - u_{ds} \cdot i_{qs} \right) \quad (10)$$

There exist two alternatives for setting the P_g reference. Hence, the RSC can drive the DFIG at the maximum power point tracking (MPPT) control mode, or otherwise follow a given reference value externally ordered [22,28]. This second alternative gains

interest when generation below the optimal operating point of the wind turbine is necessary.

On the other hand, the GSC maintains the DC bus voltage of the DFIG ($V_{dc\ DFIG}$) close to its reference, while controlling the reactive power exchange through this converter (Q_{gsc}) by acting on the *dq* grid current. The DC bus voltage is regulated by preserving the active power balance in the DC bus capacitor, which can be expressed as a function of P_r and the GSC active power (P_{gsc}), as in Eq. (11).

$$P_r - P_{gsc} = C \cdot \frac{dU_c}{dt} \cdot V_{dc\ DFIG} \tag{11}$$

where C is the capacity; and U_c the voltage at the DC link capacitor.

The GSC active power flow can be expressed as a function of the *dq* voltage and current at the AC side of the converter, u_{dqg} and i_{dqg} respectively, as given in Eq. (12).

$$P_{gsc} = 1.5 \cdot \left(u_{dg} \cdot i_{dg} + u_{qg} \cdot i_{qg} \right) \tag{12}$$

When the *d*-axis of the reference frame is oriented along the grid voltage vector, P_{gsc} can be expressed as directly dependent on u_{dg}. Subsequently, as deduced from Eq. (11), the DC bus voltage can be controlled by acting on u_{dg}. This corresponds to the upper control loop of the scheme shown in Fig. 2b.

The GSC controller was completed with the expression for Q_{gsc}, which is expressed as follows.

$$Q_{gsc} = 1.5 \cdot \left(u_{qg} \cdot i_{dg} - u_{dg} \cdot i_{qg} \right) \tag{13}$$

This reactive power depends directly on i_{qg}, and thus on u_{qg}. As a result, the control strategy for Q_{gsc} is implemented through this parameter, as illustrated in Fig. 2b.

The control strategies applied to the RSC and GSC can be achieved with a double PI-based control loop, where the outer control loop regulates the desired variable (i.e. P_g and Q_s in the RSC, and $V_{dc\ DFIG}$ and Q_{gsc} in the GSC), and the inner loop contains the current regulator. The full control scheme of these converters is shown in Fig. 2a-b.

Fig. 2. Control schemes for: (a) RSC; and (b) GSC.

In order to improve the fault ride-through capabilities of the wind turbine, the DFIG is equipped with a double active crowbar protection system located at the RSC and the DC bus [29]. This configuration protects these devices against rotor windings over-current and DC bus over-voltages, respectively, when grid disturbances occur.

3.3. Energy Storage Systems ESS (BESS and UC)

As mentioned previously, the hybrid system includes two different ESSs (BESS and UC). Commercially available devices were taken into account in their modelling, and in fact, the discharge curves provided by the manufacturers were used to validate their adequate performance.

The MATLAB/SimPowerSystems library [30] presents a lead-acid electrochemical battery model based on a variable voltage source in series with an equivalent internal resistance, which is used in the hybrid system. This model calculates the battery instantaneous voltage (U_{batt}) as a function of several design parameters and the actual operating conditions of the device according to Eq. (14).

$$U_{batt} = E_{batt} - R_i \cdot i_{batt} \tag{14}$$

where E_{batt} is the no-load voltage; R_i stands for the internal resistance of the battery; and i_{batt} is the instantaneous battery current. The no-load voltage differs between the charging and discharging process of the battery, and it depends on the battery current, the extracted capacity and hysteresis phenomenon of the battery during the charge and discharge cycles.

The battery SOC (SOC_{BESS}) is a relevant magnitude monitored in the active power SCS, which is calculated as in Eq. (15):

$$SOC_{BESS}(\%) = 100 \cdot \left(1 - \frac{\int i_{batt}\, dt}{CAP}\right) \tag{15}$$

where CAP is the maximum battery capacity; and t stands for time.

A commercially available valve-regulated lead–acid (VRLA) cell was chosen in order to obtain the required design parameters of the models. The manufacturer Discover Energy Corp. provides the information and curves for the D121000BD cell [31] that was used in this work. A comparison between the manufacturer data and the model response is shown in Fig. 3a in order to prove the adequate performance of the modeled battery. This figure shows the response of a single cell, since it was not possible to obtain from the manufacturer specific characteristics of larger cell arrays.

Following the previous model description, a total of 3 parallel-connected branches with 288 series-connected cells each are implemented in the hybrid system, achieving a

BESS rated capacity of 100 kWh with a nominal voltage of 576 V. They are connected at the DFIG output terminals via DC/DC and DC/AC converters, as shown in Fig. 1.

In the literature, different UC models can be found. Here, a reduced model was considered, which consists of a capacitor and resistance series branch. This configuration is commonly regarded as a valid option for hybrid systems [32,33]. The instantaneous UC voltage (U_{UC}) using this model is given by Eq. (16).

$$U_{UC} = U_{UC\_0} - \frac{I_{UC}}{C_{UC}} \cdot t - R_{UC} \cdot I_{UC} \tag{16}$$

where U_{UC_0} is the initial UC voltage; R_{UC} and C_{UC} are the resistance and capacity characteristics of the UC respectively; and I_{UC} is the current through the UC series branch.

Additionally, the SOC of the UC can be expressed as a function of the rated UC voltage (namely SOC_{UC} and $U_{UC\ rated}$ respectively), as in Eq. (17).

$$SOC_{UC}(\%) = 100 \cdot \frac{U_{UC}}{U_{UC\ rated}} \tag{17}$$

Moreover, the UC model was tested against a real device in order to validate its performance. The UC chosen for this purpose is the BMOD0063 P125, from the manufacturer Maxwell Technologies [34]. Fig. 3b illustrates the comparison between a constant current discharge simulation of the modeled device, and the data provided by the UC manufacturer. As seen, the model reproduces accurately the performance of the real element.

In order to accomplish a rated capacity of 2.5 kWh and a maximum voltage of 625 V at full charge, a UC bank of 5 series elements and 4 parallel branches was considered. Similarly to the BESS, DC/DC and AC/DC power converters are necessary in order to couple the UC bank to the output terminals of the DFIG. This configuration can be observed in the scheme presented in Fig. 1.

Fig. 3. Discharge curves: (a) Battery Cell D121000BD, and (b) UC BMOD0063 P125.

The design of a control strategy for the power converters implemented on both ESSs is also imperative. Here, the same control structure was considered for the BESS and UC. A single PI-based control loop allows controlling the ESSs active power output in the DC/DC converters, which are driven by a duty cycle generator, as seen in Fig. 4. Furthermore, the AC/DC converters for the ESSs, shown in Fig. 1 operate analogously to the GSC of the DFIG. Therefore, the main purpose was to maintain the DC voltage at the link between both converters close to the reference value, as well as to follow the reactive power reference provided by the SCS. As a consequence, the control strategy depicted in Fig. 2b for the GSC was also implemented on the AC/DC converters for BESS and UC.

4. Supervisory control system (SCS)

In global terms, the hybrid system consists of three main power sources, the DFIG-driven wind turbine, the BESS and the UC bank. The DFIG exchanges both active and reactive power with the grid via the stator and GSC. Therefore, it is necessary to design and implement a SCS that constantly checks the operating conditions of each component and sets the power references according to their availability and the grid

requirements. This SCS establishes independently the active and reactive power references for each power source. Hence, both control structures are depicted separately below.

4.1. Active Power SCS

The implementation of two ESSs with different characteristics in the hybrid system offers a wide variety of possibilities regarding the control strategy to apply. Among the main features of BESS, slower dynamics and higher energy density compared to UC can be highlighted, whereas the UC shows a faster response and lower capacity [8]. This must be taken into account when the SCS is designed to calculate the active power reference of both devices, as illustrated in Fig. 4.

Fig. 4. Global scheme of the active power SCS.

Firstly, three parameters are evaluated in order to set the primary active power references: the grid power demand (P_{dem}), actual DFIG active power generation (P_g), and active power generation prediction (*Power Prediction*). The latter is calculated from previous wind speed estimation and the DFIG power curve. Wind speed estimation has been addressed in the literature, and it is not studied in this paper. Therefore, the active power prediction was considered as a known external input. The main purpose of using an active power prediction is to make the wind turbine operator able to provide a time-ahead generation curve, thus resembling the operation of traditional power plants. Since the power prediction for a wind turbine is highly unlikely to be 100% accurate, ESSs help compensating the resulting error, thus ensuring the forecasted active power. On the other hand, the DFIG active power generation is calculated as the total active power

output of the DFIG, whereas the grid power demand is imposed by the grid requirements and cannot be controlled.

A thorough observation of the characteristics of these three input signals was performed in order to choose an adequate control strategy for the ESSs. Hence, the grid power demand can switch between different values, either above or below the DFIG rated power, and then remain stable in the same reference for a certain period of time. On the contrary, the DFIG active power generation changes according to the wind speed fluctuations. Regarding the active power prediction, its variability depends on the time period chosen for the wind speed estimation. In this work, an hourly mean wind speed prediction is considered as in [13], therefore the active power prediction remains unaltered during this interval.

If the wind speed estimation is adequate, the difference between the active power prediction and its actual value, which is given by the DFIG active power generation, is expected to be small and rapidly fluctuating. These properties match with the characteristics of the UC, which shows a fast response and low energy capacity. Thus, the UC bank primary active power reference is set as the difference between the active power prediction and the actual DFIG total active power generation. With this concept, the sum of the UC and DFIG active power output will equal the active power prediction as long as the SOC of the UC remains within acceptable values, thus increasing the capacity of the hybrid system to provide and comply with a forecasted power generation curve.

On the other hand, both the grid demand and the active power prediction are expected to remain stable for long intervals. Furthermore, the grid demand can differ notably from the actual DFIG generation, thus demanding a high capacity of the ESSs

to store/release energy for long periods. This performance can be achieved with the use of BESSs, since they will not be subjected to frequent and fast changes in the power reference, and they show a higher energy capacity compared to UCs. Hence, the primary active power reference for the BESS is calculated as the difference between the grid active power demand and the given active power prediction. This allows the hybrid system to supply and adapt to uncontrolled changes in the grid demand, similarly to traditional power plants, provided that the BESS stays within its recommended SOC limits.

During the exploitation of ESSs in hybrid systems, it is crucial to draw special attention to the SOC of these elements. Depending on the configuration and principle of operation of the ESS, certain maximum and minimum values of SOC should not be exceeded under the risk of damaging the device. So far, this aspect was not taken into account in the SCS developed. Hence, an innovative concept is proposed here, which implements a modification on the previously described control strategy in order to regulate the SOC of the UC and BESS.

The proposed methodology uses the primary active power references calculated previously as a function of P_{dem}, P_g and *Power Prediction*; and determines a compensating parameter that accomplishes the SOC regulation. Therefore, the measurements of the actual SOC of the ESSs are also required as inputs. The compensating parameter is presented in the form of an additional active power component that flows directly from the UC bank to the BESS, named $P_{exchange}$. This is a virtual power component, since it does not flow physically between these devices. More accurately, it consists in an additional active power term that is added to the UC and BESS primary active power references in the same amount with opposite sign. Hence,

the ESSs are required to produce an additional power injection/absorption according to the actual SOC of both ESSs and the instantaneous operating conditions.

A fuzzy logic controller was used to implement this compensating power term in the active power SCS. This fuzzy controller uses the primary active power references calculated for the UC and BESS, as well as their SOC. Regarding these inputs, the compensating power ($P_{exchange}$) is obtained as output from the fuzzy controller, and then added to the primary UC reference, and subtracted to the BESS primary power reference. This fact gives the idea of a virtual power flowing from the UC to the BESS.

The fuzzy controller operates under a list of pre-established rules, which define the status that the output signals must present regarding the level of input signals. As a result of an experience-based design procedure, the following levels were adopted for the input and output signals:

- Three possible levels were implemented for the SOC of the ESSs, i.e.: 'High SOC', 'Normal SOC' and 'Low SOC'. ESSs must operate between a maximum and a minimum level of SOC. If the recommended SOC limits are exceeded, the storage device may suffer serious damage, thus hampering its optimal performance and reducing its expected cycle-life. Therefore, the normal range of operation for the ESSs ('Normal SOC') is considered for SOC values between the maximum and minimum recommended values, where the ESSs are able to operate safely; whereas the 'High SOC' and 'Low SOC' possibilities are proposed for risky situations.

- In order to obtain a symmetrical performance for the charge and discharge cycles of the ESSs, four possibilities were considered for the primary ESS active power references, i.e.: Deep Charge (DC), Soft Charge (SC), Soft Discharge (SD) and Deep Discharge (DD). This configuration allows differentiating between soft

charge/discharge, when the ESS is absorbing/providing a moderate level of power; and the deep charge/discharge, when the SOC varies more rapidly, thus leading to risky and potentially harmful situations.

- Five different levels were selected for the compensating active power term, i.e.: Negative High (NH), Negative Low (NL), Zero (Z), Positive Low (PL) and Positive High (PH). This configuration presents symmetrical levels for positive and negative outputs (two levels for positive and another two for negative values), apart from the zero output (when power exchange between the storage devices is not needed). As detailed in the previous description, a negative value of this magnitude represents a virtual power flow from the BESS to the UC, whereas when it is positive, the power flows from the UC to the BESS.

Following this argumentation, the rules implemented are summarized in Table 1-3, where $P\text{-}P_{UC\ ref}$ and $P\text{-}P_{BESS\ ref}$ are the primary active power references for the UC and BESS, respectively. As seen, a total of 144 rules were set in order to describe the desired performance of this controller.

Table 1. Fuzzy rules for high SOC_{BESS}.

Table 2. Fuzzy rules for normal SOC_{BESS}.

Table 3. Fuzzy rules for low SOC_{BESS}.

In a fuzzy logic controller, the levels of both the input and output signals are defined according to the membership functions. Through these, the designer is able to establish the relationship between the whole range of variation of a specific signal, and the swing of the possible levels of that signal between 0 and 1. Here, the design of the membership functions was mainly deployed in two stages. First, the previous knowledge of the

controlled systems allowed establishing a primary set of membership functions, including their number, shape and range of variation. Then, a fine adjust was performed on these primary membership functions by testing them under numerous operating conditions. Though observation of the results obtained for the controlled parameters, the number, shape and variation range of the primary membership functions were gradually modified until the desired performance was finally obtained for the fuzzy controller. As general conclusions of these experiences, it was found out that with a lower number of membership functions, the control capacity of the fuzzy controller was reduced. Thus, the behavior of the SCS did not satisfy the desired operating conditions, i.e.: the exchange power suffered sharp and sudden transitions, some SOC values were not properly observed, the Deep/Soft Charge/Discharge cycles of the ESS were not clearly differentiated, etc. On the other hand, with a larger number of membership functions, it was possible to obtain a finer adjust of the fuzzy controller output. Nonetheless, the complexity of the system and thus the computational time increased substantially. Therefore, it was not considered indispensable to increase the number of membership functions in the fuzzy logic controller, since an adequate performance was obtained with the chosen membership functions.

The membership functions set for every variable in the fuzzy controller and their implementation within the SCS scheme is shown in Fig. 4. As seen, the same membership function is used for the primary active power reference inputs of the UC and BESS.

With the rules and the membership functions, the performance of the fuzzy controller is completely defined. The compensating power term is thus calculated and added/subtracted to the primary power reference. This virtual power will help

maintaining the SOC of both ESSs between adequate operational margin, while they accomplish the active power prediction and grid demand.

Finally, an additional term is considered for the UC power reference that compensates the slower dynamics of the BESS. Prior to the exportation of the power references, the maximum ESS current is limited to avoid excessive charge/discharge rates of these elements. After that, both the UC and BESS active power references are obtained from the SCS and inputted to their respective DC/DC converter controllers.

4.2. Reactive Power SCS

In order to fulfill the variable reactive power grid demand, the SCS developed for the hybrid system also manages the reactive power exchange among the different components and the grid. This is done through a proportional strategy, in which each element contributes to the grid supply with a portion of its reactive power available capacity. Hence, the first step must be to determine the reactive power limits of every device.

As previously stated, the DFIG is able to exchange reactive power through the stator windings and the GSC. The stator reactive power limitations were calculated as in [35], as a function of the DFIG operating conditions and design parameters. According to the procedure described in [35], there exist three limiting factors for the DFIG stator reactive power that must be taken into account, i.e., rotor current, rotor voltage and stator current. The aim is to obtain the PQ curves of the DFIG for each of these parameters. These can be drawn through (18)-(20), where *S* stands for apparent power, *V* for voltage, *I* for current, *Z* for impedance and *slip* is the DFIG slip; whereas subscript *s* means stator, *r* rotor and *m* mutual. Hence, variables S_{s_Ir}, S_{s_Vr} and S_{s_Is} are the stator

apparent power according to the rotor current, rotor voltage and stator current limitations.

$$S_{s\_Ir} = -U_s \cdot U_s^* \cdot \left(\frac{1}{Z_s + Z_m} \right)^* + I_r^* \cdot U_s \cdot \left(\frac{Z_m}{Z_s + Z_m} \right)^* \tag{18}$$

$$S_{s\_Vr} = -U_s \cdot \left(\frac{U_s \cdot (Z_r + Z_m) - \frac{U_r}{slip} \cdot Z_m}{(Z_r + Z_s) \cdot Z_m + Z_s \cdot Z_r} \right)^* \tag{19}$$

$$S_{s\_Is} = -U_s \cdot I_s^* \tag{20}$$

These equations were programmed in an embedded function in the MATLAB/Simulink hybrid system model. For every given operating condition, the previous set of equations provides three positive and three negative values of the stator apparent power. The lowest absolute values of the positive and negative results are then chosen as the stator reactive power consumption and generation limits respectively.

For the GSC, UC and BESS, the calculation of the limits is much simpler compared to the DFIG stator. In all the three cases, the reactive power flows through an AC/DC converter, together with an active power term. Hence, the reactive power capability of these converters is given by (21), where Q_{conv} is the available reactive power capacity, S_{conv} is the rated apparent power, and P_{conv} is the active power, referred to the respective AC/DC converters.

$$Q_{conv} = \pm\sqrt{S_{conv}^2 - P_{conv}^2} \tag{21}$$

As seen in Eq. (21), both positive and negative values are obtained for Q_{conv}, thus being the consumption and generation limits of the converter.

Once the grid requirements and the available reactive power capacity of all the elements are known, the SCS calculates a proportional distribution between the four reactive power sources of the hybrid system, according to their limits. This proportional distribution must be accomplished taking into account the entire consumption or generation capacity of the hybrid system, as well as the grid demand. This can be achieved through Eqs. (22)-(23). As seen, Eq. (22) shows solely the calculation of the reactive power reference for the DFIG stator (Q_{s_ref}). It is expressed as a function of the stator reactive power consumption limit ($Q_{s\_con\_lim}$), the reactive power grid demand (Q_{dem}), which in Eq. (22) corresponds to reactive power consumption in the hybrid system, and the total reactive power consumption limitation ($Q_{con\_lim\_total}$), which is given by the sum of the stator, GSC, UC and BESS limits, as shown in Eq. (23).

$$Q_{s\_ref} = \frac{Q_{s\_con\_lim}}{Q_{con\_lim\_total}} \cdot Q_{dem\ (con)} \tag{22}$$

$$Q_{con\_lim\_total} = Q_{s\_con\_lim} + Q_{gsc\_con\_lim} + Q_{UC\_con\_lim} + Q_{BESS\_con\_lim} \tag{23}$$

The same strategy as in Eq. (22) was applied to the other components of the hybrid system (GSC, UC and BESS converters), and for the reactive power generation case, where the opposite limitations are considered. With this scheme, every element in the system absorbs/supplies a value of reactive power proportional to its available capacity. Therefore, the reactive power grid requirements will be completely fulfilled through the different power sources as long as they remain below the total capacity of the hybrid system.

5. Simulations and Discussion

The adequate performance of the SCS designed was tested by simulation in MATLAB/Simulink under different situations. The main objective is to prove the proper regulation of the SOC of both ESSs by action of the fuzzy controller, while being able to address the grid active and reactive power requirements. Furthermore, grid disturbances were also considered, and the hybrid system response to a voltage sag is shown.

In cases study I and II, the analysis focuses on the performance of the active and reactive power, and SOC management of the SCS. The time frame chosen for these simulations is 60 s. In principle, a 60 s-long simulation might seem a short simulation interval in order to observe substantial changes in a large-scale battery. Nonetheless, the main objective of the simulations presented is to show the proper operation of the developed control systems, i.e.: active and reactive power SCSs, and power converters controllers. These control systems are responsible for calculating the adequate references for the DFIG and storage devices that allow addressing the grid demand and balancing the errors in active power prediction. Also, the fuzzy controller implemented on the active power SCS maintains the SOC of the ESSs within recommended values. All these features are clearly shown throughout the simulations performed herein. Moreover, two 60 s-long simulations have been carried out with the aim of studying two different situations (normal and low) for the SOC of the BESS. The conclusions drawn from these two simulations are analogous to those that could be obtained from a longer simulation in which the SOC of the BESS varied slowly. Therefore, the interest of these cases study is not focused on the simulation time, but stressed on analyzing a varied set of different operating conditions within the time frame chosen for the simulations. Hence, since the main characteristics of the hybrid system can be successfully analyzed

within the simulation period selected, a longer simulation time is not considered necessary.

Therefore, three different control strategies are compared. First, the complete active power SCS with fuzzy logic developed in Section 4.1 is evaluated. Its response is compared with the same structure without the fuzzy logic compensator, that is to say, the primary active power references are directly inputted to the ESSs power controllers without SOC compensation. Lastly, an alternative control strategy for SOC management is also illustrated for comparison purposes. This control scheme applied on the SCS is based on a state machine implemented through a truth table in MATLAB/Simulink. The state machine receives the primary active power references for BESS and UC as inputs, and provides two power references, one for each ESS, modified according to the SOC of the storage devices. This configuration avoids exceeding the maximum and minimum recommended SOC limits for BESS and UC. More details regarding the state machine SCS can be found in [22].

On the other hand, in case study III, the response and recovery of the hybrid system to voltage sags at the point of common coupling (PCC) to grid is addressed. During voltage sags, it is crucial to achieve a proper reactive power flow to the grid with the aim of supporting the voltage recovery. Hence, in this simulation a comparative analysis is performed between the configuration with and without the reactive power scheme implemented on the SCS. In both cases, the active power SCS operates with the fuzzy controller, since the active power regulation within the elements in the hybrid system is not the key factor in this situation.

5.1. Case study I: Normal SOC in both ESSs

In this first simulation, normal operation of the hybrid system is shown. Strongly fluctuating wind speed is inputted to the model, which varies between 8 and 20 m/s. This wind time series was obtained through a Weibull distribution, using a variable mean speed value, and adding a random term to include the natural turbulence of wind. The resulting wind speed profile is shown in Fig. 5a.

The grid active and reactive power demand also changes along the simulation according to the illustration in Fig. 5b. The active power demand is fixed at 1 pu, 0.7 pu and 1.2 pu at different times during the simulation, whereas the reactive power demand varies from -0.6 pu to 0.45 pu with a slope of 0.1 pu/s at 30 s.

Fig. 5. Case Study I: (a) Wind speed profile, (b) Active and reactive power grid demand, (c) DFIG active power generation, and (d) total active power output.

The ability of the active power SCS to address the grid requirements, as well as to regulate the SOC of both ESSs, with and without the fuzzy logic controller, and with the state machine SCS, was tested and compared in this case study.

The DFIG active power generation for the three control strategies in the SCS is shown in Fig. 5c. The DFIG generation prediction is also represented. This value was set at 0.85 pu during the simulation. Hence, the prediction remains either above or below the actual DFIG generation during different intervals, thus changing the sign of the primary active power reference for the UC.

As seen in Fig. 5c, the active power DFIG generation depends on the incoming wind speed to the wind turbine. Furthermore, given the external connection of the ESSs, the

control strategy implemented in the SCS does not affect the normal operation of the DFIG, since the response obtained in all cases is similar.

The total output power provided by the hybrid system represented in Fig. 5d illustrates the effect of the ESSs. These devices allow the hybrid system to address the active power grid requirements regardless the actual wind conditions, as long as their SOC remains between adequate values. Therefore, the total active power output switches from 1 pu to 0.7 pu, and then to 1.2 pu as the grid demand changes. Certain difference between the configurations can be seen at 35 s, when the SCS with the fuzzy controller shows a faster response. This is due to a higher active power injection of the UC compared to the case without the fuzzy controller or the state machine.

The active power flow through the ESSs is shown in Fig. 6a-b. As stated before, the SCS intended to exploit the main qualities of each ESS, shorter response time in the UC and larger energy capacity of BESS. In Fig. 6a, it can be seen that the UC is required to perform frequent and fast changes in its active power output, switching repeatedly between charge and discharge operation. These fluctuations correspond to the error observed between the wind power prediction (hourly mean constant value) and the actual generation, which varies with the incoming wind. Hence, the UC is controlled in order to ensure that the sum of its output power and the DFIG generation (plus the compensating power $P_{exchange}$ in the configuration with fuzzy controller) equals the power prediction at all times, thus allowing the hybrid system to accomplish the forecasted generation.

On the other hand, the variation of the BESS active power (Fig. 6b) is less abrupt and with fewer changes in the sign, what leads to longer charge/discharge cycles compared to the UC. Indeed, the UC active power presents 18 changes in the sign (switches

between charge/discharge), whereas only 6 were registered in the BESS active power for the SCS with fuzzy logic in this 60 s-long simulation (only 2 for the schemes without fuzzy and the state machine). This stable performance is preferred for the BESS, given its slower response time and in order to reduce the impact of a switching output power on the cycle life of the battery. The smoother power supply accomplished on the BESS is a consequence of the primary active power control strategy designed for the BESS, which compensates the differences between the grid demand and the power prediction. This power mismatch does not show a highly fluctuating behavior, since only occasional variations are expected in both signals. However, this power imbalance can be large and maintained for long periods. Therefore, high capacity ESSs, such as large-scale batteries, are more suitable than UCs for this purpose. This smart control strategy optimizes the overall response of the hybrid system by considering the main characteristics of the ESSs.

Fig. 6. Case Study I: (a) UC active power, (b) BESS active power, and (c) compensating active power term.

Considerable differences can be noticed in Fig. 6a-b between the SCS with fuzzy controller and the other two alternatives. These differences are due to the compensating active power term calculated by the fuzzy controller, which is illustrated in Fig. 6c under the label $P_{exchange}$.

As previously detailed, the main purpose of the fuzzy controller is to regulate the SOC of the ESSs by means of the active power $P_{exchange}$, which by definition flows virtually from the UC to the BESS. Fig. 6c shows that $P_{exchange}$ becomes negative in some periods when the BESS stores energy (between 10 s and 35 s), thus leading to

higher charge in the UC and lower charge in the BESS compared to the case in which the fuzzy controller is not implemented or the state machine is utilized on the SCS. On the other hand, when the BESS is discharged to meet the grid demand, the UC supports the BESS, thus achieving lower charge and deeper discharge cycles in the UC, and lower discharge in the BESS. The UC support to the BESS during approximately the second half of the simulation corresponds to positive values of the compensating term $P_{exchange}$.

The benefits of the fuzzy controller on the regulation of the SOC of the ESSs can be appreciated in Fig. 7.

Fig. 7. Case Study I: (a) UC SOC, and (b) battery SOC.

Remarkable differences can be found in this parameter because of the use of the fuzzy controller. In the three cases, the UC starts the simulation at the same SOC, and the responses remain identical as long as $P_{exchange}$ is zero. At 10 s, the UC SOC starts to increase by action of $P_{exchange}$ when the fuzzy controller is included in the SCS, and it shows a rising tendency throughout the whole simulation. On the other hand, the SCS without fuzzy does not take into account the SOC in order to generate the active power reference. Therefore, the UC SOC remains lower than the case with fuzzy controller from 10 s until the simulation finishes. For the state machine SCS, the SOC resembles the response observed in the SCS without fuzzy logic, since the primary active power reference is only modified by the state machine when the SOC of the ESSs is close to the limit recommended values, which does not occur in this simulation. This behavior differs from the compensation power concept developed with the fuzzy controller. By the end of the simulation, the SOC of the case with fuzzy controller is 23% higher

compared to the SCS without fuzzy or state machine regulation, reaching a maximum difference of 60% at 32 s. These results prove the improvement achieved with the fuzzy controller in the SOC of the UC.

Regarding the BESS SOC, all SCS configurations show the same response up to 10 s, when the BESS starts to provide an extra active power injection in order to support the UC. As a consequence, between 10 s and 35 s, the SOC decreases approximately a 0.2% in the case with fuzzy controller, whereas it increases a 0.8% when the fuzzy controller is not implemented, or the state machine is used. On the other hand, from 35 s up to the end of the simulation, the SOC with the fuzzy controller decreases only a 2.7%, whereas in the alternative configurations the SOC reduction in this period is 3.3%. This lower decrease in the SOC is due to the UC support to the BESS through the compensating term $P_{exchange}$ during the second half of the simulation.

As seen, the addition of the fuzzy controller in the SCS has a very positive effect on the UC SOC, while it does not hamper the proper operation of the BESS.

The SCS is also responsible for setting the reactive power references of the different elements in the hybrid system with the aim of addressing the grid requirements. In Fig. 8, the total output, as well as stator, GSC, UC and BESS responses are shown. As observed, the reactive power output of every element varies according to its current operating conditions. It can be highlighted that the total output matches the reactive power grid demand throughout the simulation, thus proving the adequate performance of the SCS. Moreover, no relevant differences are observed between the SCS with and without fuzzy controller, nor with the state machine configuration. Hence, the implementation of the fuzzy logic controller does not affect significantly the reactive power response of the hybrid system.

Fig. 8. Case Study I: (a) Total reactive power output, (b) stator reactive power, (c) GSC reactive power, (d) UC converter reactive power, and (e) BESS converter reactive power.

In this case study, the hybrid system was able to fulfill the active and reactive power grid demand through the whole simulation, while improving the response of the UC SOC with the implementation of the fuzzy controller.

5.2. Case Study II – Low SOC in BESS

This second case study analyses the performance of the hybrid system under a situation of low SOC in the BESS. The active and reactive power grid requirements have been maintained at the same levels as in case study I (Fig. 5). Fig. 9a shows the wind speed profile used as input, which was obtained through a Weibull distribution with variable mean speed and random turbulence.

As illustrated in Fig. 9b-d, under the given conditions, when the fuzzy controller is present the UC is governed by the active power SCS to support the BESS through $P_{exchange}$ for long periods. Thus, the compensating power (Fig. 9d) is clearly positive as long as the BESS primary active power reference is negative (BESS discharge). Between 10 s and 35 s, the primary active power reference for the BESS becomes positive, thus $P_{exchange}$ decreases and varies close to zero.

Fig. 9. Case Study II: (a) Wind speed profile, (b) UC active power, (c) BESS active power, and (d) compensating active power term.

In Fig. 9b-c, the UC and BESS active power responses are illustrated. It can be observed that relevant differences appear from 0 s to 10 s, and from 35 s to 60 s

between the three alternatives, as a result of the $P_{exchange}$ generated by the fuzzy controller to regulate the SOC of the ESSs. Regarding P_{UC} in Fig. 9b, the fuzzy controller generates $P_{exchange}$ (Fig. 9d) so that the UC supports the charge of the BESS, which registers low SOC in this simulation, with an additional active power injection. Opposite, in the schemes without fuzzy controller and with state machine, the UC only compensates the power mismatch between power prediction and generation, thus storing energy during most of the simulation. Approximately at time 59 s, the UC reaches its maximum recommended SOC (Fig. 11a). Subsequently, as can be observed in Fig. 9b, the state machine sets to zero the UC active power reference, so that this limit is not exceeded. This event is not observed in the control configuration without fuzzy controller, since the SOC of the ESSs is not assessed in this strategy.

In Fig. 9c, the state machine accomplishes the continuous charge of the BESS during the whole simulation, in order to recover from the low SOC. Nonetheless, the configuration with fuzzy controller experiences both charge and discharge cycles, due to the simultaneous necessity for supplying grid demand while avoiding excessive discharge. This can be achieved by the additional power injection provided by the UC through $P_{exchange}$. On the other hand, the configuration without the fuzzy controller follows the primary active power reference for the BESS without taking into consideration the low SOC of this device. As a consequence, at approximately 50 s, the BESS experiences terminal voltage decrease and its power supply reduces to zero.

The compensating power $P_{exchange}$ calculated by the fuzzy controller is shown in Fig. 9d. As seen, this power is virtually extracted from the UC and driven to the BESS in order to moderate its low SOC.

Furthermore, the most relevant improvement achieved with the implementation of the fuzzy controller is depicted in Fig. 10a. At approximately 50 s, the SCS without fuzzy controller is not able to address the grid requirements. Since the BESS SOC is not regulated, the battery voltage drops below the operating limits of this device, and its active power injection decreases (as observed in Fig. 9c). Subsequently, the total active power output diminishes and the grid demand is unattended. With the fuzzy controller, the BESS SOC is supervised, and the grid requirements can be fulfilled along the whole simulation. Therefore, the inclusion of the fuzzy controller in the SCS can be the difference between meeting or not the active power grid demand under certain circumstances. Regarding the state machine SCS, the grid demand is unaddressed as long as it remains above the forecasted generation, since this situation requires BESS discharge, which is unfeasible given the state machine regulation. At 59 s, the UC ceases storing the power imbalance between prediction and generation, and thus the total active power output increases to 0.96 pu, still below the grid requirements.

Fig. 10. Case Study II: (a) Total active power output, and (b) total reactive power output.

The SOC control performed by the fuzzy controller has been a crucial feature of the hybrid system to properly meet the grid demand in this simulation. Fig. 11 illustrates the SOC of UC and BESS. Contrarily to the previous simulation, the UC SOC, in the cases without fuzzy controller or with state machine, remains higher than the SCS with fuzzy controller throughout this case study. Nonetheless, without the fuzzy controller the UC SOC increases uncontrolled, and surpasses 100% by the end of the simulation, which is not the optimal situation, since the maximum voltage constrain of the UC is exceeded.

The state machine is able to stop the SOC of the UC at 100% by setting its active power reference to zero when this value is recorded. Furthermore, even though the UC shows a higher SOC, the hybrid system is not able to completely supply the demanded active power in the cases without fuzzy or with state machine SCS, thus wasting this stored energy from the grid operation point of view.

Fig. 11. Case Study II: (a) UC SOC, and (b) battery SOC.

On the other hand, the BESS SOC with the fuzzy controller increases above the case without fuzzy. This is due to the support of the UC, which helps maintaining the BESS within adequate operating conditions throughout the simulation, thus enhancing the performance of the hybrid system when the fuzzy controller is implemented. A higher BESS SOC increase is observed for the state machine SCS, since the battery charges continuously during the whole simulation. However, this charge is accomplished at the expense of the total active power output, which is not able to fulfill the grid demand during most of this case study.

Finally, the total reactive power output is shown in Fig. 10b. In this case, all configurations prove a satisfactory response and are able to address the variable grid demand. As in the previous simulation, the total reactive power output is accomplished by the proportional participation of all the devices in the hybrid system.

5.3. Case Study III – Response to voltage sag

In this simulation, a voltage sag of 0.2 pu at PCC with a 0.5 s duration is studied and represented in Figs. 12-13. It corresponds to the most severe situation that wind farms must be able to ride through according to the current Spanish grid code [36]. Constant wind speed was considered in order to focus only on the electric dynamics of the

system. Moreover, the configurations with and without reactive power SCS are compared, in order to show the improvements achieved with the proposed reactive power control strategy. Regarding the active power SCS, the scheme including the fuzzy controller was used in both cases.

First, the total reactive power generation is shown in Fig. 12b. As seen, the hybrid system with reactive power SCS is able to provide a reactive power injection of 0.9 pu during the voltage sag. This can be achieved through the stator winding of the DFIG, as well as the GSC, BESS and UC converters. When the reactive power management is removed from the SCS, these devices do not receive an adequate reactive power reference. Hence, the controllers operate to maintain the zero reactive power exchange with the grid. Moreover, it can be seen that the reactive power consumption peak after the fault clearance is remarkably lower in the case of the reactive power SCS compared to the situation when this block is not implemented (0.4 pu vs. 1 pu respectively).

Fig. 12. Case Study III: (a) Total active power output, and (b) total reactive power output.

One of the main advantages of a superior reactive power injection during this grid disturbance can be clearly observed in Fig. 13a. As a consequence of the generated reactive power, in the model without the reactive power SCS, the wind farm voltage drops to 0.2 pu during the voltage sag, whereas if the supervisory controller is implemented, the voltage is maintained at 0.4 pu, thus achieving a remarkable improvement. This higher voltage reduces the effects in the wind farm output terminals of this severe voltage sag at PCC.

Fig. 13. Case Study III: (a) Hybrid system output voltage, (b) DFIG DC bus voltage, (c) BESS DC bus voltage, and (d) UC DC bus voltage.

The active power generation during the voltage sag also improves when the reactive power SCS operates (Fig. 12a). Since the voltage drop is mitigated by this controller, the active power response is also enhanced, showing an injection to grid of 0.4 pu by the end of the sag, whereas the model without reactive power SCS registers a 0.18 pu active power generation in this interval.

Therefore, the reactive power SCS designed improves the fault ride through of the hybrid system with two ESSs, as a consequence of the higher active and reactive power generation achieved.

Finally, the voltage at the DFIG and at the DC bus of the BESS and UC converters is shown in Fig. 13b-d. It can be observed that in all the cases the DC voltages remain close to their references either before, during and after the fault, for both the configurations with and without reactive power SCS, by action of the respective controllers and protections. This DC voltage response is an indicator of the electric stability in the whole system during this grid disturbance.

The better operation of the hybrid model with reactive power SCS has been proved along this case study, where the system was submitted to a severe voltage sag and an improved performance was accomplished.

6. Conclusions

This paper has presented and evaluated a wind hybrid system composed of a DFIG wind turbine equipped with BESS and UC. Taking into account the main characteristics

of these energy storage devices, a SCS was designed and implemented. This SCS operates independently the active and reactive power references for each component. The active power SCS considers the fast response of UCs and large capacity of BESS to calculate a primary reference based on active power generation, prediction and demand. This reference is later modified by a fuzzy logic controller depending on the SOC of the ESSs and the fuzzy rules specified. This strategy allows maintaining the SOC of both ESSs between adequate operative margins.

On the other hand, the reactive power SCS delivers a proportional reference as a function of the grid demand and the actual limitations of each element of the hybrid system, thus avoiding potentially harmful situations.

The wind hybrid system with two ESSs was simulated under different operating conditions, including variable wind speed and grid demand, and grid disturbance (voltage sag). Three different control strategies were compared: 1) SCS with fuzzy logic controller; 2) SCS with the same structure as the first SCS but without the fuzzy logic controller; and 3) SCS based on state machine control.

Results showed that the SCS with fuzzy logic controller achieved better energy management between the power sources in order to address the grid requirements, while maintaining the SOC of the ESSs within recommended values. Moreover, the reactive power SCS showed an improved performance under grid disturbances, enhancing the voltage recovery and higher active and reactive power injection to grid during voltage sags.

Acknowledgements

This work has been supported by the University of Cadiz under the Grant FPI 2012-036, by the Spanish Ministry of Science and Innovation under Grant ENE2010-19744/ALT, and by the Foundation Technological Campus of Algeciras.

References

[1] Beaudin M, Zareipour H, Schellenberglabe A, Rosehart W. Energy storage for mitigating the variability of renewable electricity sources: An updated review. Energy Sustain Dev 2010;14(4):302-14.

[2] Carton JG, Olabi AG. Wind/hydrogen hybrid systems: Opportunity for Ireland's wind resource to provide consistent sustainable energy supply. Energy 2010;35(12):4536-44.

[3] Gutiérrez-Martín F, Da Silva-Álvarez RA, Montoro-Pintado P. Effects of wind intermittency on reduction of CO2 emissions: The case of the Spanish power system. Energy 2013:61:108-17.

[4] Lopes Ferreira H, Garde R, Fulli G, Kling W, Pecas Lopes J. Characterisation of electrical energy storage technologies. Energy 2013:53:288-98.

[5] General Electric Company. Products & Services: 2.5-120 Wind Turbine. Available from: http://www.ge-energy.com/products_and_services/products/wind_turbines/ges_2.5_120_wind_turbine.jsp [accessed July 12, 2013].

[6] Ferreira HL, Garde R, Fulli G, Kling W, Lopes JP. Characterisation of electrical energy storage technologies. Energy 2013;53:288-98.

[7] Hadjipaschalis I, Poullikkas A, Efthimiou V. Overview of current and future energy storage technologies for electric power applications. Renew Sustain Energy Rev 2009;13(6–7):1513-22.

[8] Evans A, Strezov V, Evans TJ. Assessment of utility energy storage options for increased renewable energy penetration. Renew Sustain Energy Rev 2012;16(6):4141-7.

[9] Carro-Calvo L, Salcedo-Sanz S, Kirchner-Bossi N, Portilla-Figueras A, Prieto L, Garcia-Herrera R, et al. Extraction of synoptic pressure patterns for long-term wind speed estimation in wind farms using evolutionary computing. Energy 2011;36(3):1571-81.

[10] Liu H, Shi J, Erdem E. Prediction of wind speed time series using modified Taylor Kriging method. Energy 2010;35(12):4870-9.

[11] Guo Z, Zhao J, Zhang W, Wang J. A corrected hybrid approach for wind speed prediction in Hexi Corridor of China. Energy 2011;36(3):1668-79.

[12] Hong Y-Y, Chang H-L, Chiu C-S. Hour-ahead wind power and speed forecasting using simultaneous perturbation stochastic approximation (SPSA) algorithm and neural network with fuzzy inputs. Energy 2010;35(9):3870-6.

[13] Kavasseri RG, Seetharaman K. Day-ahead wind speed forecasting using *f*-ARIMA models. Renew Energy 2009;34(5):1388-93.

[14] Kusiak A, Zhang Z, Verma A. Prediction, operations, and condition monitoring in wind energy. Energy 2013;60:1-12.

[15] Chen D, Liu S, Ma X. Modeling, nonlinear dynamical analysis of a novel power system with random wind power and it's control. Energy 2013;53:139-46.

[16] Kamel RM, Chaouachi A, Nagasaka K. Wind power smoothing using fuzzy logic pitch controller and energy capacitor system for improvement Micro-Grid performance in islanding mode. Energy 2010;35(5):2119-29.

[17] de Almeida RG, Peas Lopes JA, Barreiros JAL. Improving power system dynamic behavior through doubly fed induction machines controlled by static converter using fuzzy control. IEEE Trans Power Syst 2004;19(4):1942-50.

[18] Pichan M, Rastegar H, Monfared M. Two fuzzy-based direct power control strategies for doubly-fed induction generators in wind energy conversion systems. Energy 2013;51:154-62.

[19] Jerbi L, Krichen L, Ouali A. A fuzzy logic supervisor for active and reactive power control of a variable speed wind energy conversion system associated to a flywheel storage system. Electr Power Syst Res 2009;79(6):919-25.

[20] Mohamed Thameem Ansari M, Velusami S. DMLHFLC (Dual mode linguistic hedge fuzzy logic controller) for an isolated wind–diesel hybrid power system with BES (battery energy storage) unit. Energy 2010;35(9):3827-37.

[21] Capizzi G, Tina G. Long-term operation optimization of integrated generation systems by fuzzy logic-based management. Energy 2007;32(7):1047-54.

[22] Sarrias R, Fernández LM, García CA, Jurado F. Coordinate operation of power sources in a doubly-fed induction generator wind turbine/battery hybrid power system. J Power Sources 2012;205:354-66.

[23] Sarrias R, Fernández LM, García CA, Jurado F. Supervisory control system for DFIG wind turbine with energy storage system based on battery. In: Proceedings of the International Conference on Power Engineering, Energy and Electrical Drives; 2011 May 11-13; Málaga, Spain.

[24] General Electric Company. Products & Services: 1.5-77 Wind Turbine. Available from: http://www.ge-energy.com/products_and_services/products/wind_turbines/ge_1.5_77_wind_turbine.jsp [accessed July 12, 2013].

[25] Heier S. Grid integration of wind energy conversion systems. John Wiley & Sons; 1998.

[26] Slootweg JG. Wind Power: Modelling and Impact on Power System Dynamics [Ph. D. Thesis] Delft University of Technology, Netherlands; 2003.

[27] Krause P, Wasynczuk O, Sudhoff SD. Analysis of Electric Machinery and Drive Systems. IEEE Press Series on Power Engineering. John Wiley & Sons; 2002.

[28] Fernández LM, García CA, Jurado F. Comparative study on the performance of control systems for doubly fed induction generator (DFIG) wind turbines operating with power regulation. Energy 2008;33(9):1438-52.

[29] Bongiorno M, Thiringer T. A generic DFIG model for voltage dip ride-through analysis. IEEE Trans Energy Convers 2013;28(1):76-85.

[30] Hydro-Québec/the MathWorks Inc. SimPowerSystemsTM. Natick, MA; 2010.

[31] Discover Energy Corp. Products Datasheets - Cell D121000BD. Available from: http://www.discover-energy.com/sites/default/files/datasheets/D121000BD.pdf [accessed July 12, 2013].

[32] Abbey C, Joos G. Supercapacitor energy storage for wind energy applications. IEEE Trans Ind Appl 2007;43(3):769-76.

[33] Wei L, Joos G, Belanger J. Real-time simulation of a wind turbine generator coupled with a battery supercapacitor energy storage system. IEEE Trans Ind Electron 2010;57(4):1137-45.

[34] Maxwell Technologies. Products Datasheets - 125 V UC Modules. Available from: http://www.maxwell.com/products/ultracapacitors/products/125v-tran-modules [accessed July 12, 2013].

[35] Lund T, Sørensen P, Eek J. Reactive power capability of a wind turbine with doubly fed induction generator. Wind Energy 2007;10(4):379-94.

[36] Spanish TSO, Red Eléctrica de España. Requirements of response against voltage sags in wind power generation facilities (P.O. 12.3) [In Spanish]. Available from: http://www.ree.es/operacion/pdf/po/PO_resol_12.3_Respuesta_huecos_eolica.pdf [accessed July 12, 2013].

LIST OF FIGURES AND TABLES

Figure 1

Click here to download high resolution image

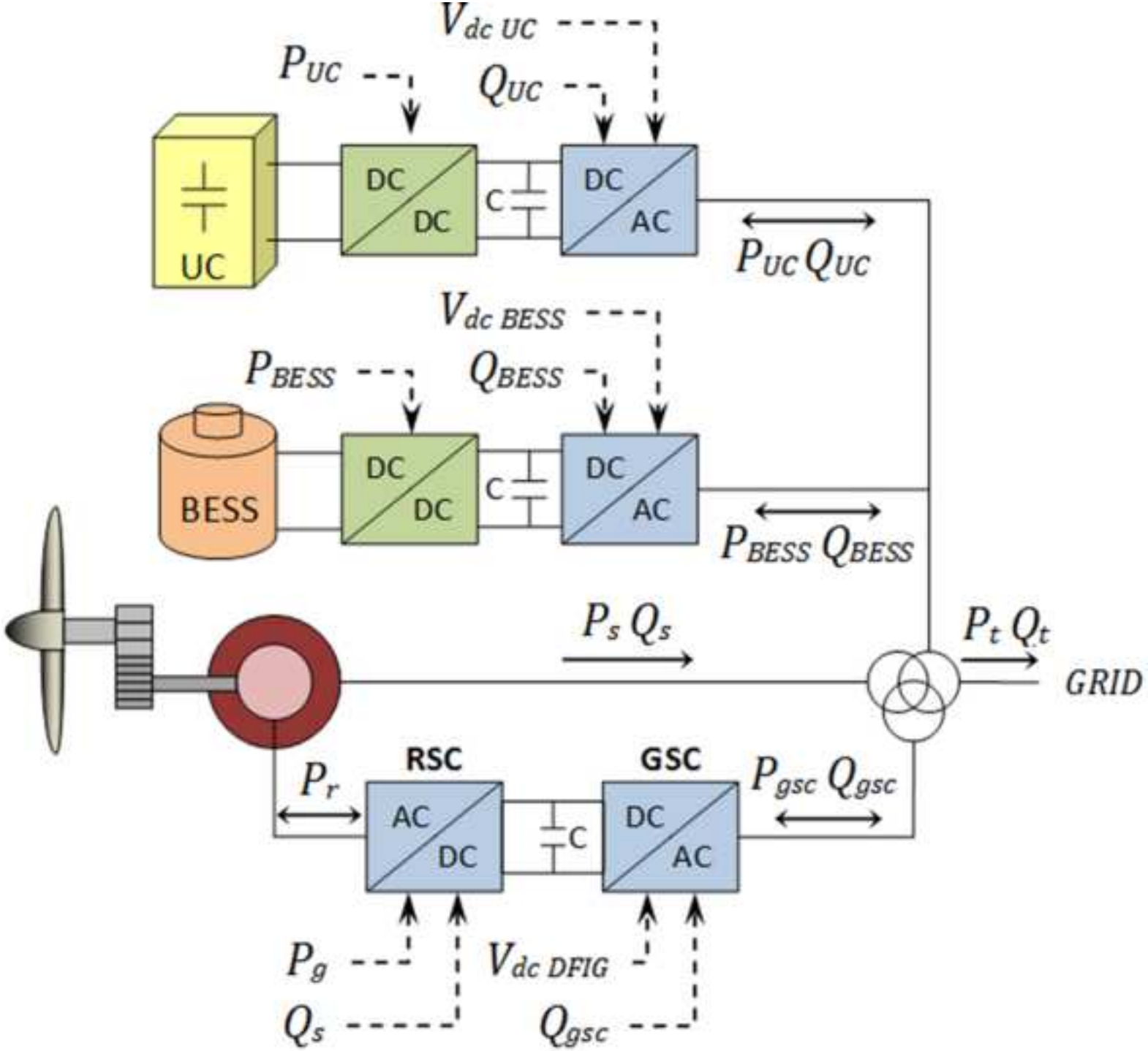

Figure 2

Click here to download high resolution image

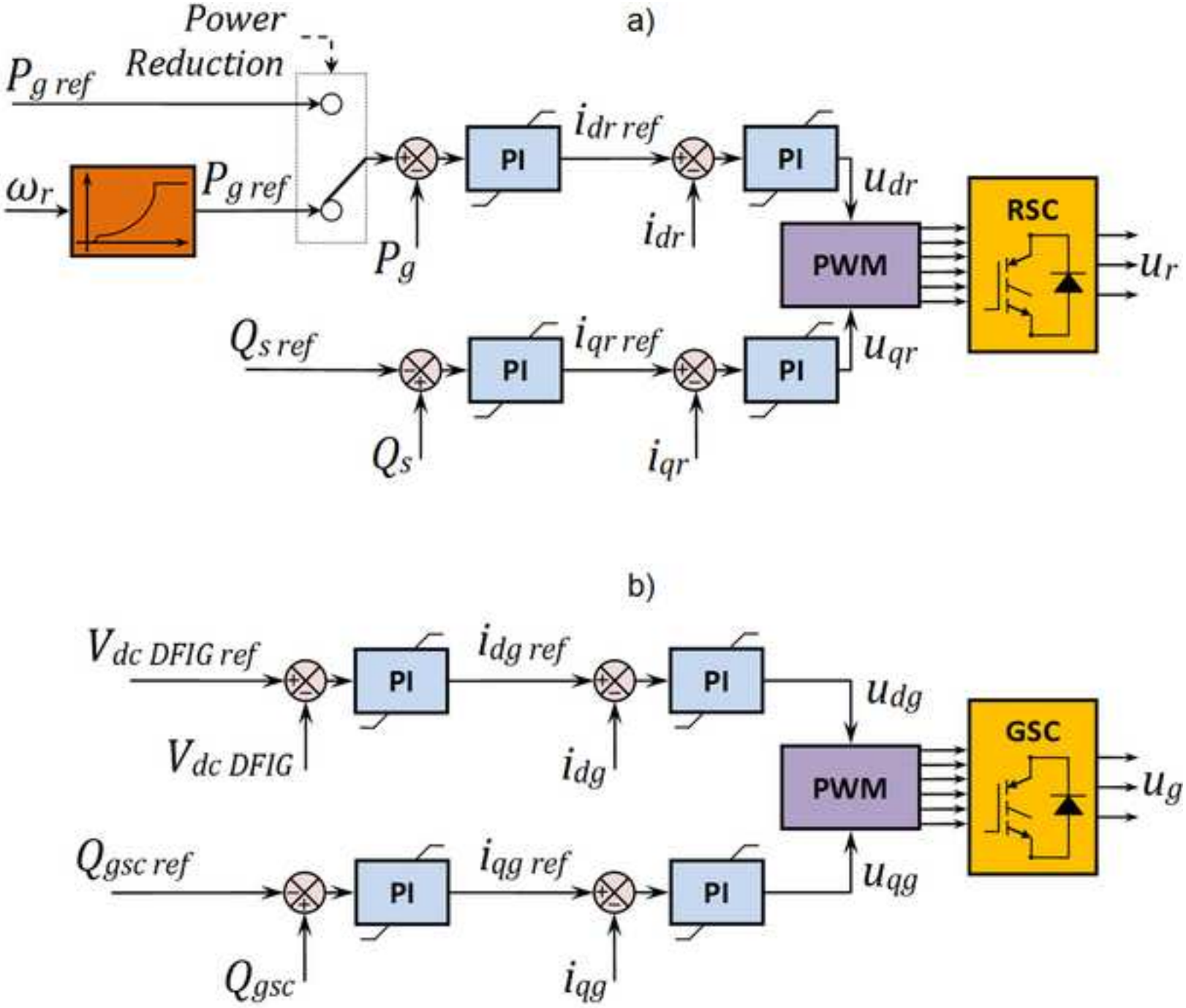

Figure 3

Click here to download high resolution image

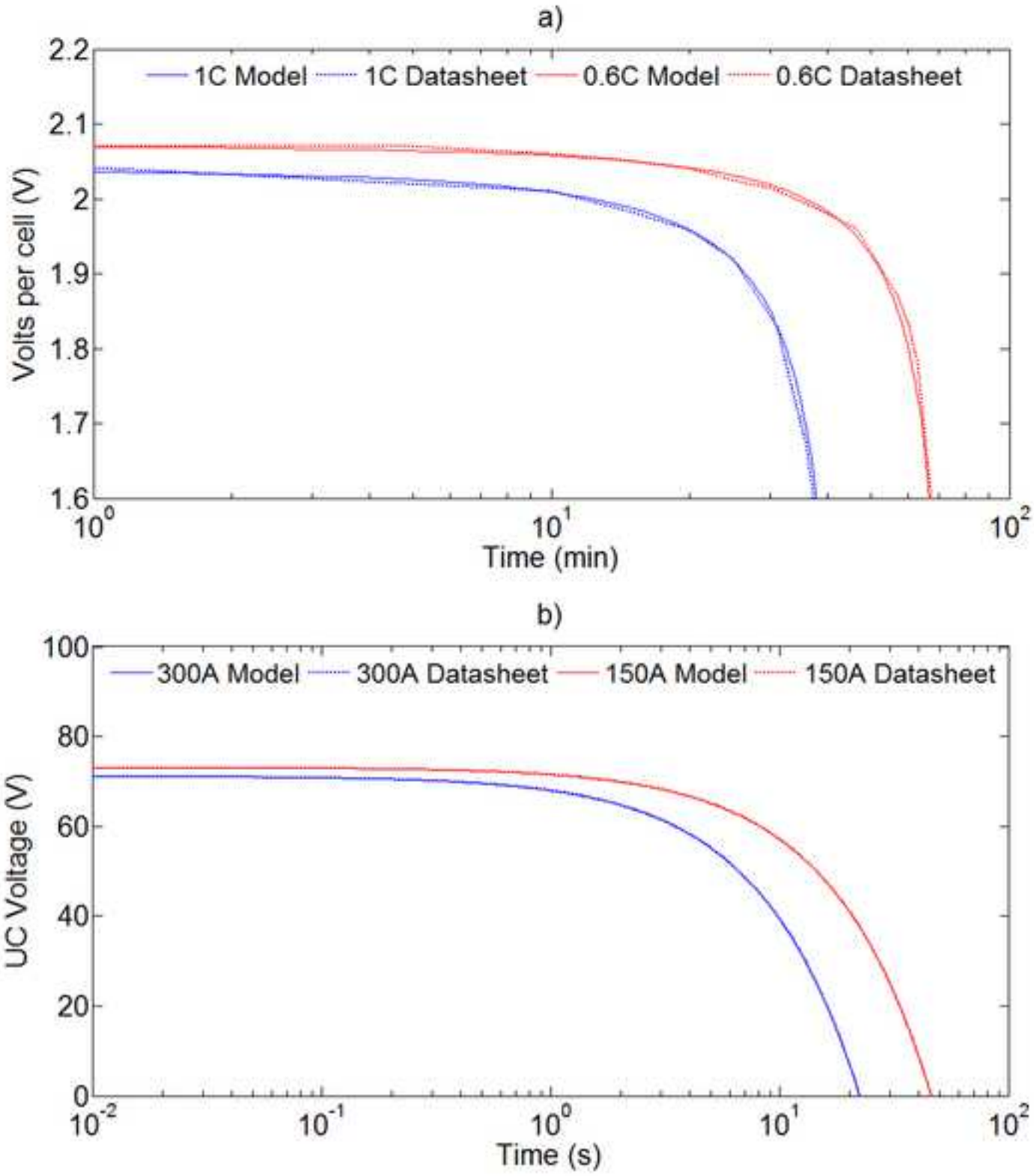

Figure 4

Click here to download high resolution image

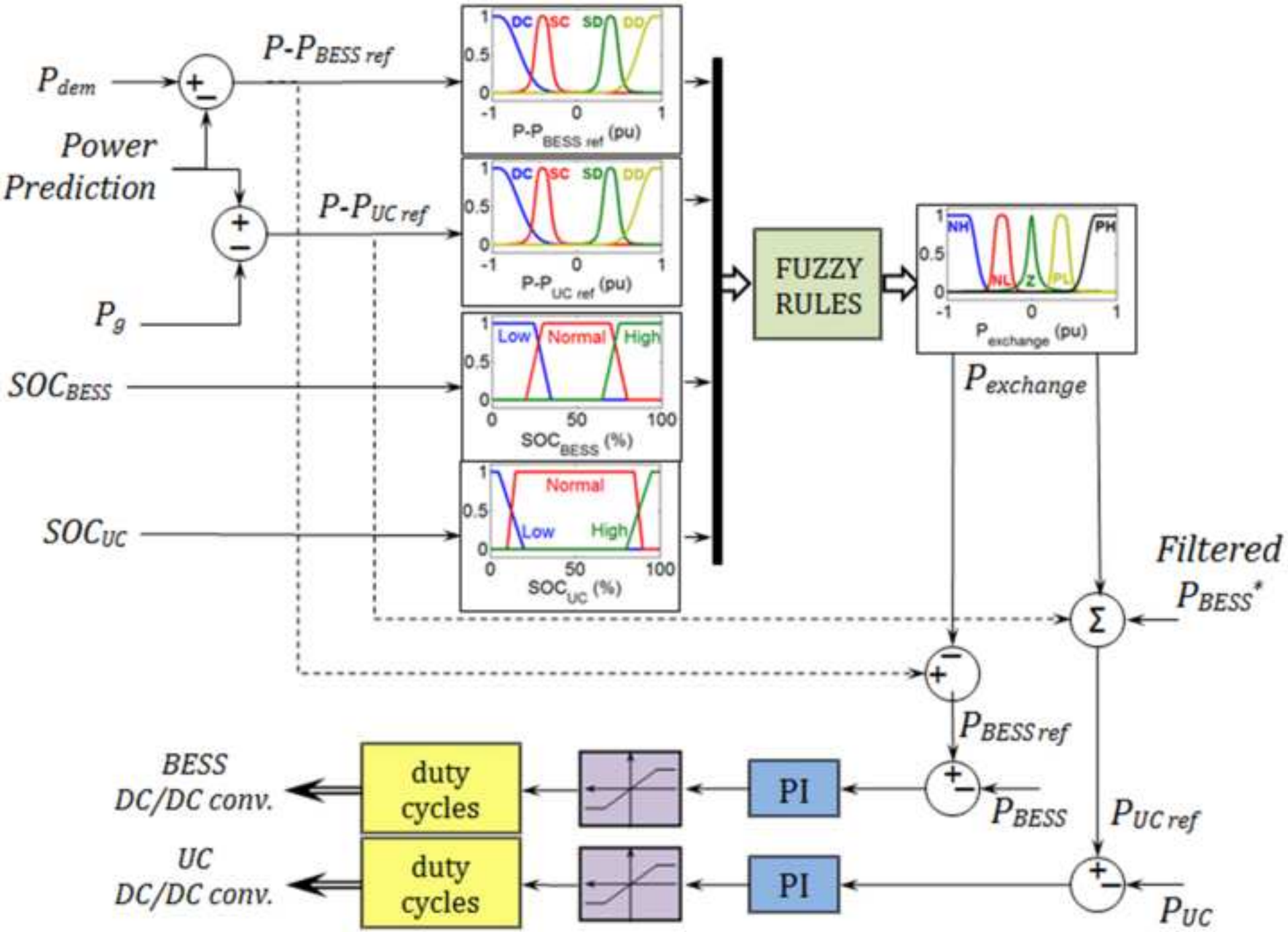

Figure 5

Click here to download high resolution image

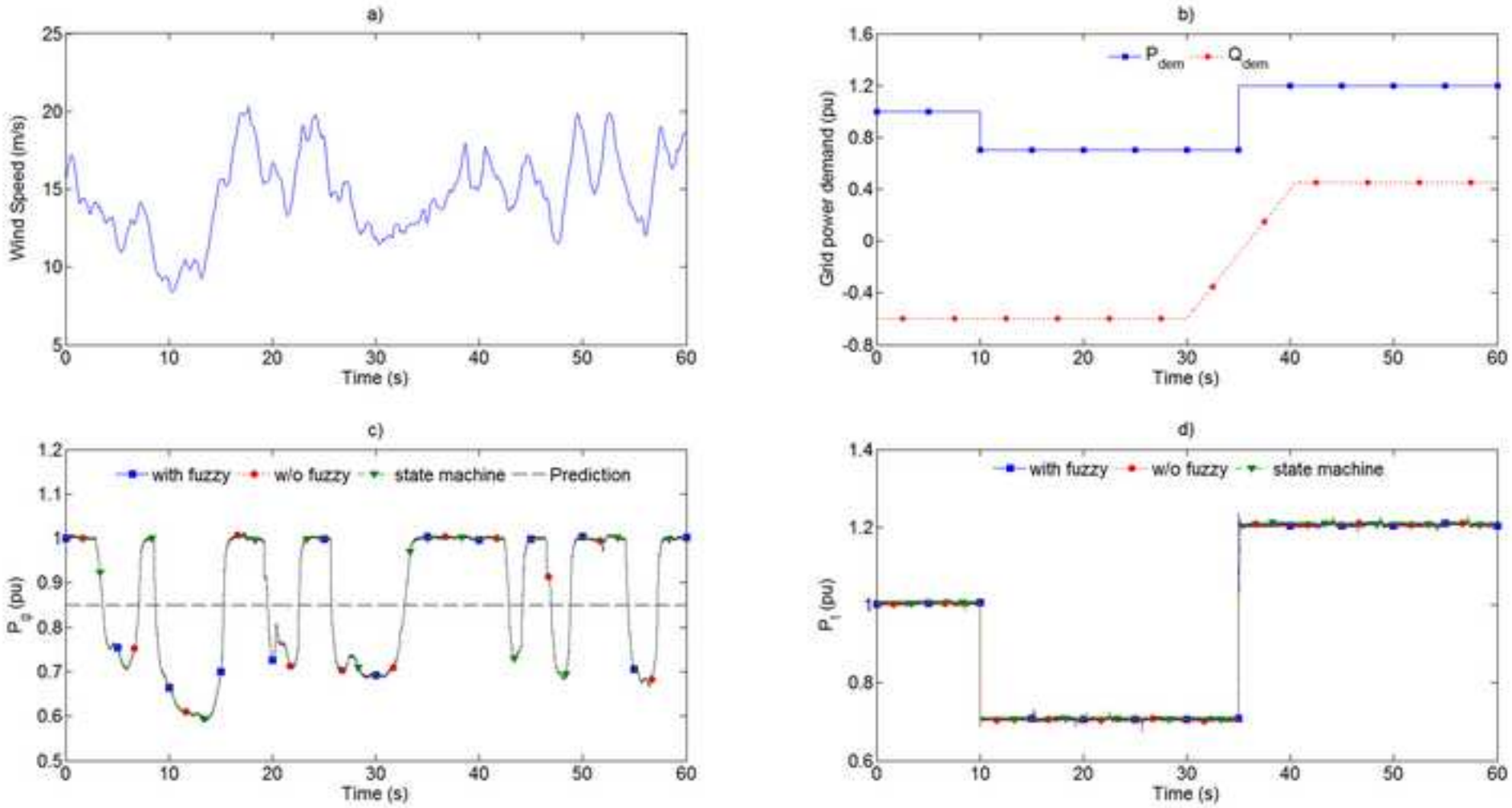

Figure 6

Click here to download high resolution image

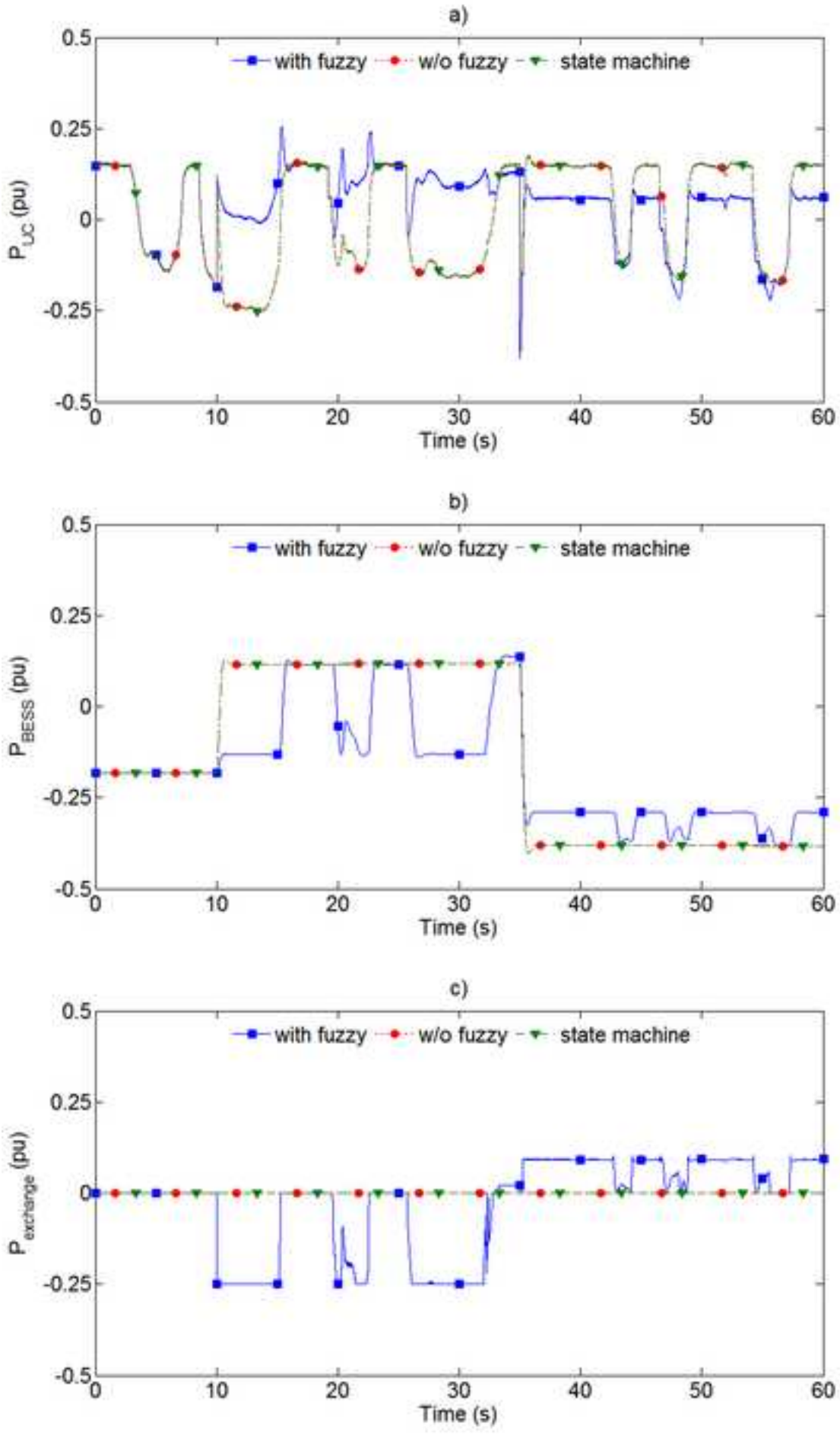

Figure 7

Click here to download high resolution image

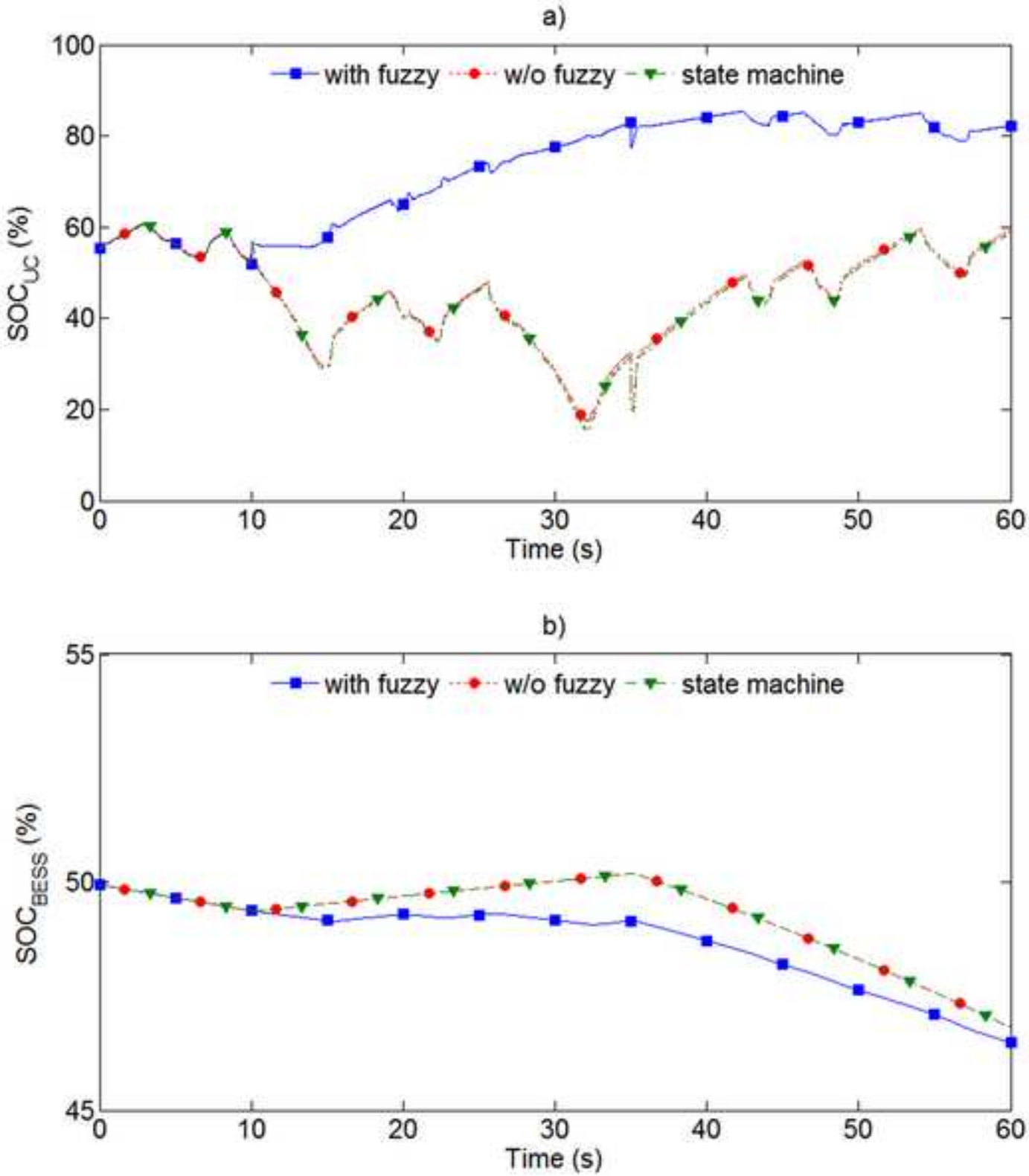

Figure 8

Click here to download high resolution image

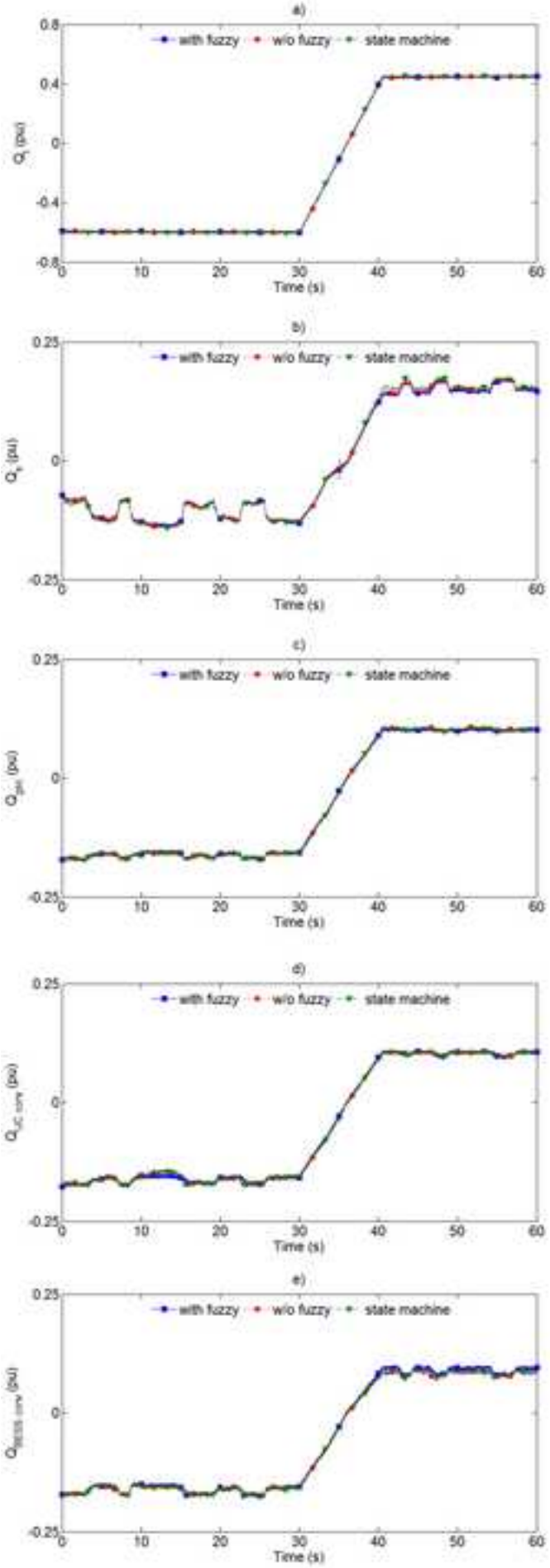

Figure 9

Click here to download high resolution image

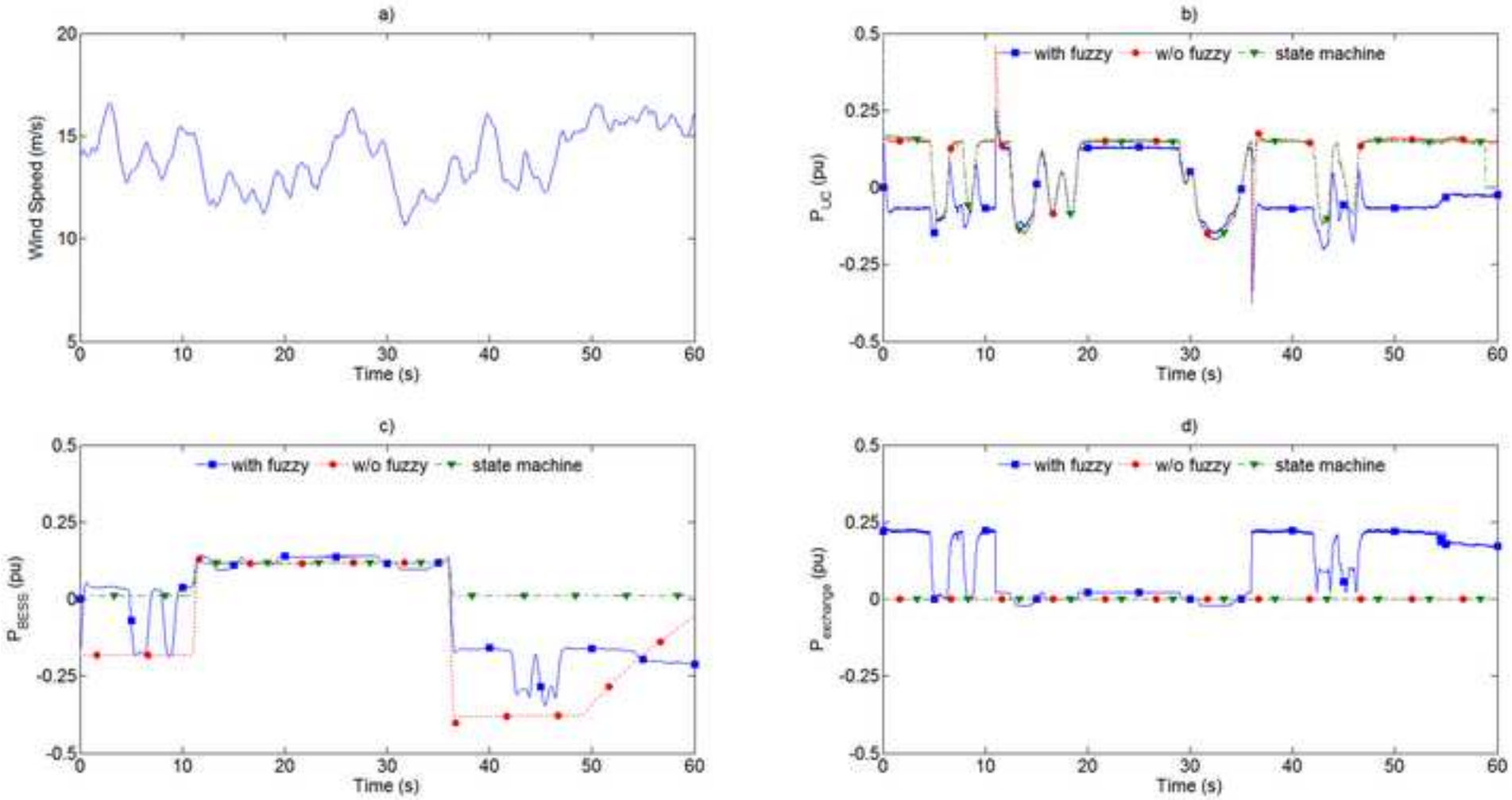

Figure 10

Click here to download high resolution image

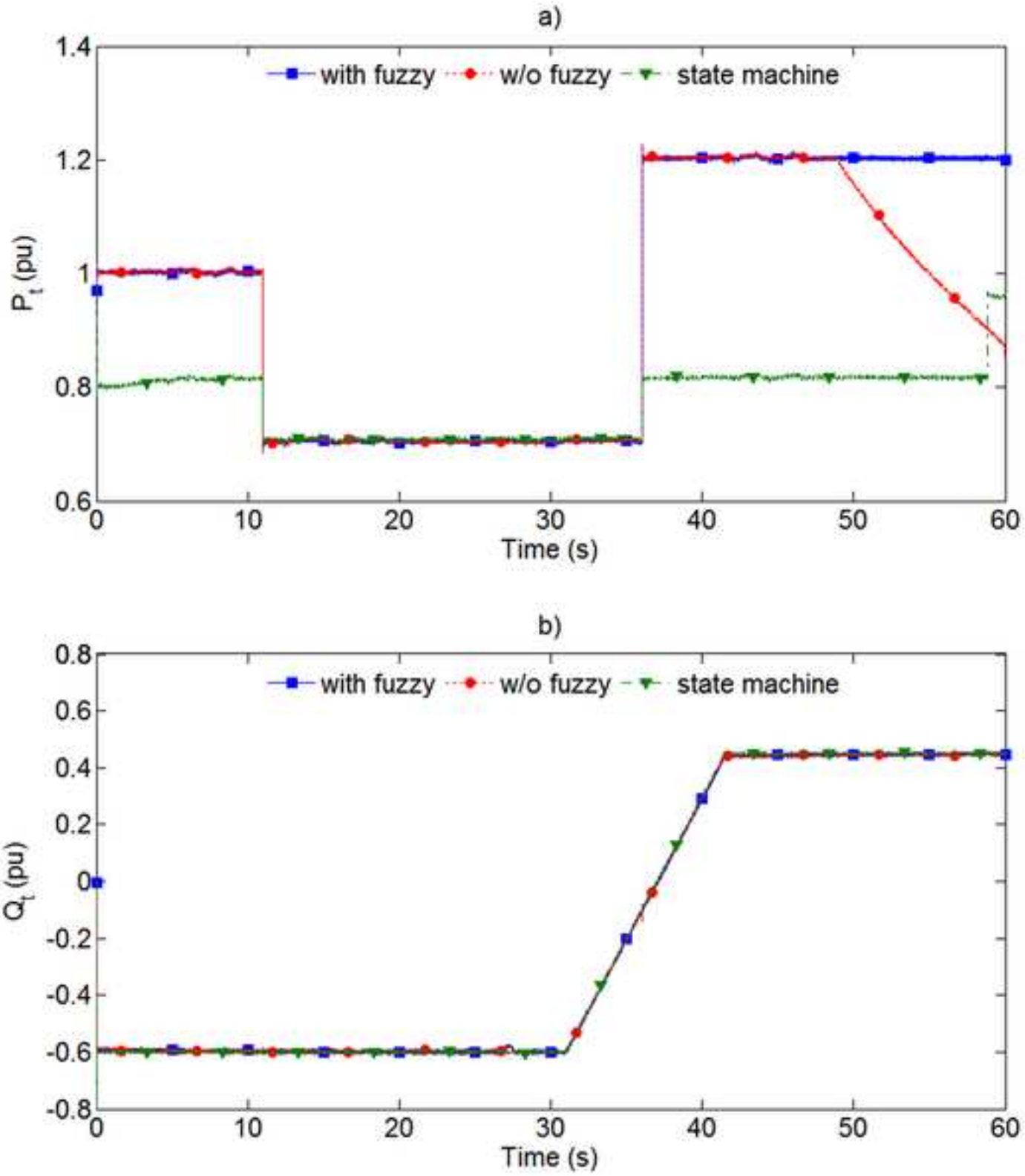

Figure 11

Click here to download high resolution image

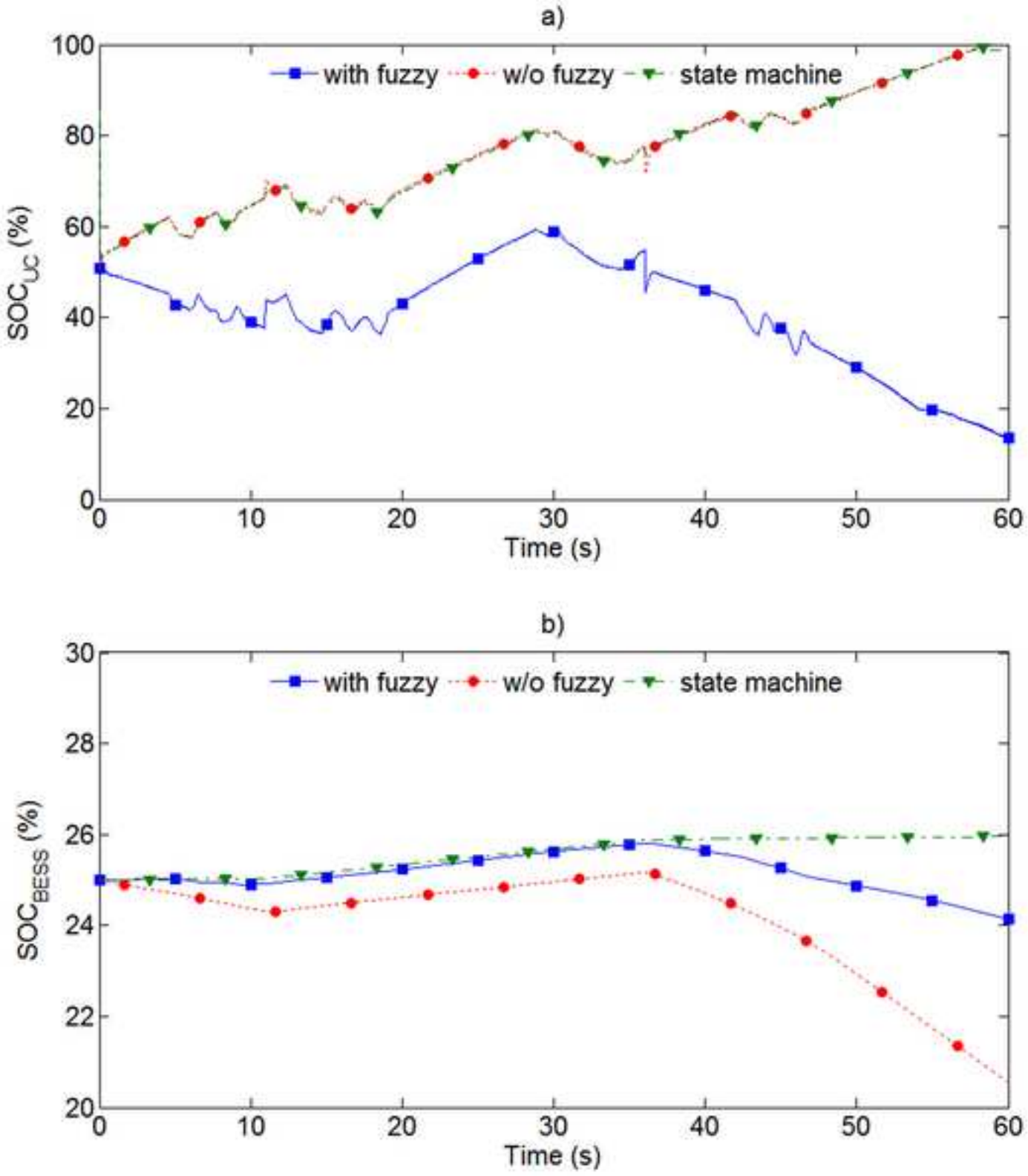

Figure 12

Click here to download high resolution image

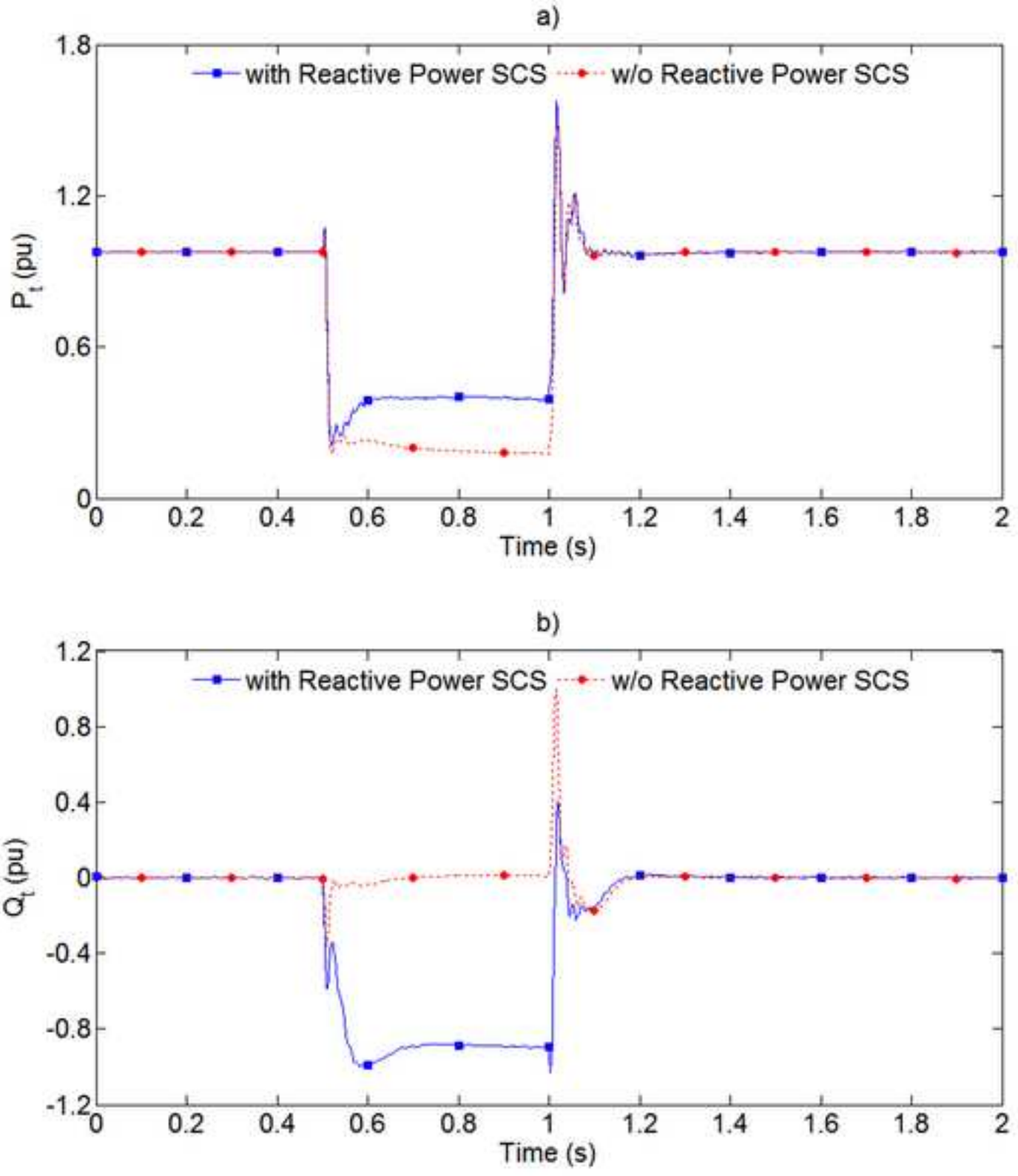

Figure 13

Click here to download high resolution image

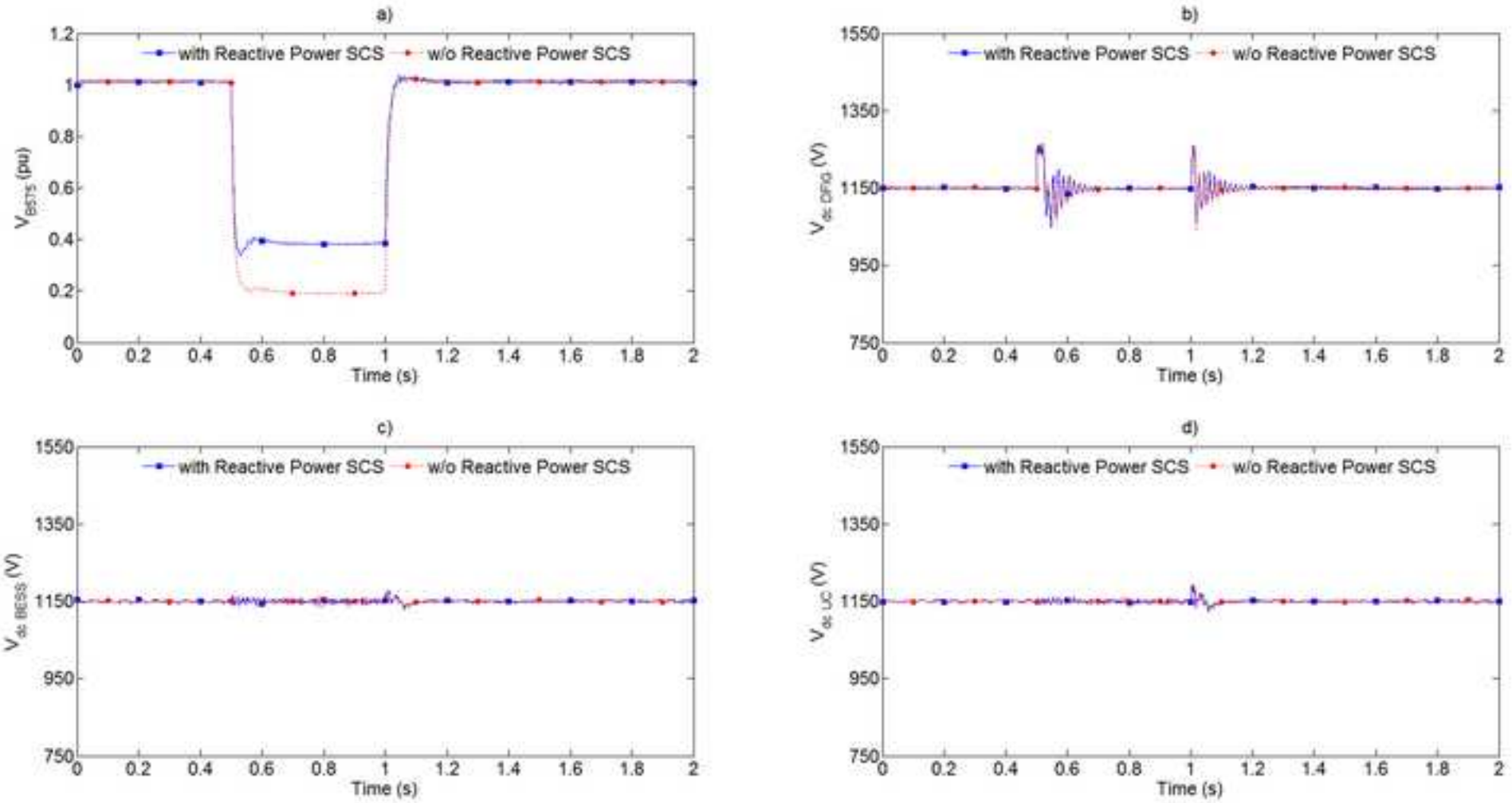

Table 1

Table 1. Fuzzy rules for high SOC_{BESS}

SOC_{BESS}: HIGH

SOC_{UC}: HIGH

$P\text{-}P_{UC\ ref}$ / **$P\text{-}P_{BESS\ ref}$**	**DC**	**SC**	**SD**	**DD**
DC	Z	Z	NL	NH
SC	PL	PL	NL	NH
SD	PH	PL	Z	NL
DD	PH	PL	Z	Z

SOC_{UC}: NORMAL

$P\text{-}P_{UC\ ref}$ / **$P\text{-}P_{BESS\ ref}$**	**DC**	**SC**	**SD**	**DD**
DC	NL	NL	NH	NH
SC	NL	NL	NH	NH
SD	Z	Z	NL	NH
DD	Z	Z	NL	NL

SOC_{UC}: LOW

$P\text{-}P_{UC\ ref}$ / **$P\text{-}P_{BESS\ ref}$**	**DC**	**SC**	**SD**	**DD**
DC	NH	NH	NH	NH
SC	NH	NH	NH	NH
SD	NL	NL	NH	NH
DD	Z	NL	NL	NH

Table 2

Table 2. Fuzzy rules for normal SOC_{BESS}

SOC_{BESS}: NORMAL

SOC_{UC}: HIGH

$P\text{-}P_{UC\ ref}$ / **$P\text{-}P_{BESS\ ref}$**	**DC**	**SC**	**SD**	**DD**
DC	PL	PL	Z	NL
SC	PL	PL	Z	NL
SD	PH	PL	PL	Z
DD	PH	PH	PL	Z

SOC_{UC}: NORMAL

$P\text{-}P_{UC\ ref}$ / **$P\text{-}P_{BESS\ ref}$**	**DC**	**SC**	**SD**	**DD**
DC	Z	Z	NL	NH
SC	Z	Z	NL	NL
SD	PL	Z	Z	NL
DD	PL	PL	Z	Z

SOC_{UC}: LOW

$P\text{-}P_{UC\ ref}$ / **$P\text{-}P_{BESS\ ref}$**	**DC**	**SC**	**SD**	**DD**
DC	NH	NH	NH	NH
SC	NL	NH	NH	NH
SD	NL	NL	NH	NH
DD	Z	Z	NL	NH

Table 3

Table 3. Fuzzy rules for low SOC_{BESS}

SOC_{BESS}: LOW

SOC_{UC}: HIGH

$P\text{-}P_{UC\ ref}$ / **$P\text{-}P_{BESS\ ref}$**	**DC**	**SC**	**SD**	**DD**
DC	PH	PL	Z	Z
SC	PH	PL	PL	PL
SD	PH	PH	PH	PL
DD	PH	PH	PH	PH

SOC_{UC}: NORMAL

$P\text{-}P_{UC\ ref}$ / **$P\text{-}P_{BESS\ ref}$**	**DC**	**SC**	**SD**	**DD**
DC	Z	Z	Z	Z
SC	PL	PL	Z	Z
SD	PH	PH	PL	PL
DD	PH	PH	PH	PH

SOC_{UC}: LOW

$P\text{-}P_{UC\ ref}$ / **$P\text{-}P_{BESS\ ref}$**	**DC**	**SC**	**SD**	**DD**
DC	Z	Z	NL	NL
SC	Z	Z	NL	NL
SD	PL	PL	Z	Z
DD	PL	PL	Z	Z